

Exploring Basic Tail Modifications of Coumarin-Based Dual Acetylcholinesterase-Monoamine Oxidase B Inhibitors: Identification of Water-Soluble, Brain-Permeant Neuroprotective Multitarget Agents

Leonardo Pisani,[†] Roberta Farina,[†] Marco Catto,^{*,†} Rosa Maria Iacobazzi,[†] Orazio Nicolotti,[†] Saverio Cellamare,[†] Giuseppe Felice Mangiatordi,[†] Nunzio Denora,[†] Ramon Soto-Otero,[‡] Lydia Siragusa,[§] Cosimo Damiano Altomare,[†] and Angelo Carotti[†]

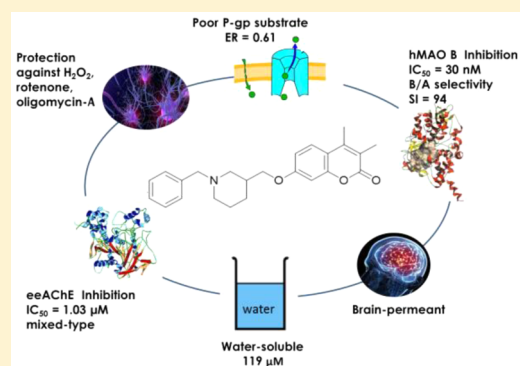
[†]Dipartimento di Farmacia—Scienze del Farmaco, Università degli Studi di Bari “Aldo Moro”, via E. Orabona 4, I-70125 Bari, Italy

[‡]Departamento de Bioquímica y Biología Molecular, Facultad de Medicina, Universidad de Santiago de Compostela, San Francisco I, E-15782 Santiago de Compostela, Spain

[§]Molecular Discovery Limited 215 Marsh Road, Pinner, Middlesex, London HA5 5NE, U.K.

Supporting Information

ABSTRACT: Aiming at modulating two key enzymatic targets for Alzheimer’s disease (AD), i.e., acetylcholinesterase (AChE) and monoamine oxidase B (MAO B), a series of multitarget ligands was properly designed by linking the 3,4-dimethylcoumarin scaffold to 1,3- and 1,4-substituted piperidine moieties, thus modulating the basicity to improve the hydrophilic/lipophilic balance. After in vitro enzymatic inhibition assays, multipotent inhibitors showing potencies in the nanomolar and in the low micromolar range for hMAO B and eeAChE, respectively, were prioritized and evaluated in human SH-SY5Y cell-based models for their cytotoxicity and neuroprotective effect against oxidative toxins (H₂O₂, rotenone, and oligomycin-A). The present study led to the identification of a promising multitarget hit compound (**Sb**) exhibiting high hMAO B inhibitory activity (IC₅₀ = 30 nM) and good MAO B/A selectivity (selectivity index, SI = 94) along with a micromolar eeAChE inhibition (IC₅₀ = 1.03 μM). Moreover, **Sb** behaves as a water-soluble, brain-permeant neuroprotective agent against oxidative insults without interacting with P-gp efflux system.



INTRODUCTION

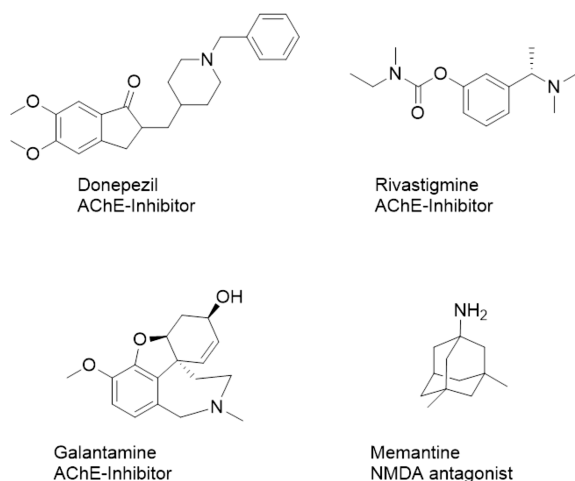
The incidence and socio-economic costs of neurodegenerative diseases (NDs) are constantly growing as a consequence of the increased life expectancy and aging population. Among NDs, a major role is played by Alzheimer’s disease (AD), representing the most common cause of dementia. As population ages, the devastating impact of AD increases worldwide, being estimated that more than 100 million individuals will suffer from AD by 2050.¹ Alzheimer’s patients experience an irreversible cognitive decline, associated with severe memory, attention, and learning deficits impairing daily life activities. In the last decades, massive investments in both academic and private settings, even though lower than in other healthcare programs (e.g., anticancer therapies), have been devoted to the discovery of novel diagnostic and therapeutic tools against AD. Unfortunately, the road to effectively treat AD with both small molecules and immunotherapies addressing amyloid as well as tau hypotheses² has been paved with failures³ even in late-stage clinical trials,⁴ and disease-modifying drugs are missing. The disheartening attrition rate has commonly been ascribed to the multifactorial

etiopathogenesis of AD exhibiting several neuronal aberrations spanning from proteostasis,⁵ metal unbalance,⁶ and oxidative stress to mitochondrial dysfunctions,⁷ ultimately leading to disruption of cholinergic transmission in hippocampus and frontal cortex.⁸ It is still a matter of debate whether researchers are addressing the wrong targets and/or the disease models are not appropriate.

So far, with the exception of memantine (approved in 2003),⁹ the restoration of basal neurotransmitter acetylcholine (ACh) levels through acetylcholinesterase (AChE) inhibitors (Chart 1; donepezil, galantamine, and rivastigmine) is the only approved, albeit palliative, therapeutic strategy in mild forms of AD.¹⁰ In more recent years, the research shifted to the more promising multitarget strategy,¹¹ rooted on the principle that a combination of actions may be beneficial for multifactorial pathologies including AD¹² by hitting two or more relevant targets with the same molecular entity.^{13,14} In many anti-

Received: April 13, 2016

Chart 1. Approved Drugs for AD (Common Name, Mechanism of Action)



66 Alzheimer multitargeting programs, chelation of biometals,¹⁵
67 agonism to 5-HT₄ receptors,¹⁶ antagonism to 5-HT_{1A}
68 receptors,¹⁷ radical scavenging,¹⁸ and release of vasodilating
69 NO radical^{19,20} have been considered valuable biochemical
70 activities that could synergistically improve the therapeutic
71 potential of AChE inhibition often remaining the core feature
72 of multipotent agents.

73 AChE (EC 3.1.1.7) is a serine hydrolase responsible for the
74 deacetylation of ACh in both central and peripheral nervous
75 system.²¹ A 20 Å narrow tunnel, chiefly lined by aromatic
76 residues, separates a catalytic anionic site (CAS),²² close to the
77 catalytic triad, from another anionic subsite (peripheral anionic
78 site, PAS) that binds the cationic heads of gorge-spanning dual
79 binding site (DBS) inhibitors and acts as chaperone-like motif
80 during the formation of Aβ oligomers.²³ Another ChE isoform
81 (butyrylcholinesterase, BChE, EC 3.1.1.8)²⁴ has the same
82 biological function, and its inhibitors may also have impact in
83 the therapy of AD²⁵ because its activity increases in advanced
84 AD forms.²⁶ To alleviate oxidative stress conditions of
85 degenerating neurons, the inhibition of MAO (amine-oxygen
86 oxidoreductase; EC 1.4.3.4) activity might be addressed.²⁷ This
87 flavoenzyme catalyzes the degradation of endogenous and
88 xenobiotic amines (including many neurotransmitters as
89 catecholamines and serotonin) and contributes to increase
90 reactive oxygen species (ROS) level through its catalytic cycle
91 by producing the corresponding aldehyde metabolite and
92 hydrogen peroxide as the end products. The two known
93 isoforms, termed MAO A and MAO B,^{28,29} differ in amino acid
94 sequences, tissue distribution, and selectivity for substrates and
95 inhibitors. As far as the role of MAO in AD is concerned, the
96 potential application of MAO inhibitors in therapy needs to
97 address a crucial selectivity issue. In fact, strong dietary
98 restrictions³⁰ are required to avoid unwanted side effects³¹
99 associated with the blockade of peripheral MAO A by
100 nonselective inhibitors. Moreover, MAO B predominates in
101 brain tissue and its activity increased in the elderly, especially in
102 glial cells.³²

103 As a part of our ongoing research on multifunctional ligands
104 against NDs,^{17,33} we recently devoted our efforts to the
105 identification of coumarin-based AChE-MAO B inhibitors with
106 improved drug-like properties.³⁴ Among privileged hetero-
107 cycles, the coumarin core has been extensively decorated by
108 several research groups addressing the discovery of novel

selective MAO^{35–39} and AChE^{40–42} inhibitors as well as to
build new molecular scaffolds with dual AChE-MAO activity⁴³
against NDs, in most cases through a conjugative approach.^{44,45}
Over the past decade, our contribution to this field highlighted
the important role of substituents at position 4 and 7 of
coumarin in tuning MAO B activity and selectivity.^{46–50} Aiming
at obtaining multipotent compounds with good overall
pharmacokinetic properties, we herein focused on modifica-
tions of the basic head of the side chain at C7 and of the spacer
connecting the two key pharmacophore features (namely the
basic head and the coumarin core) in order to improve aqueous
solubility while maintaining a dual AChE-MAO B inhibitory
activity. Starting from a potent multi-target directed ligand
(MTDL),³⁴ the new molecular framework was built as depicted
in Figure 1. The lipophilic phenyl ring was removed from the

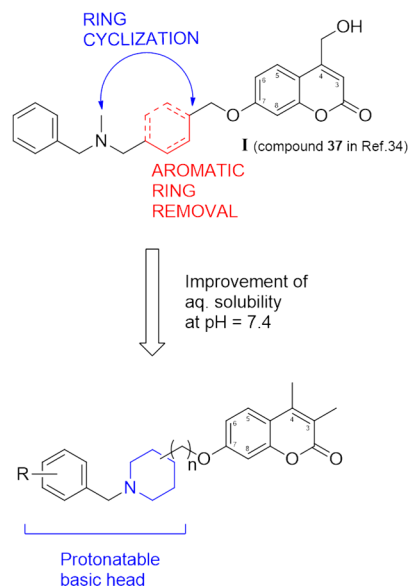


Figure 1. Rational design.

spacer, and the basic nitrogen was enclosed in a flexible
piperidine cycle, thus modulating the pK_a of N-sp³ and the
aqueous solubility at physiological pH. By approaching this
ring-closing strategy around the basic nitrogen, we conceived a
series of 2H-chromen-2-ones bearing a donepezil-inspired
benzylpiperidine moiety that may efficiently interact with
AChE binding pocket.⁵¹ 3,4-Dimethylcoumarin was exploited
as a molecular fragment to enhance MAO B affinity because
this scaffold proved to be efficiently accommodated in the
lipophilic enzymatic pocket that faces the FAD coenzyme and is
unable to lodge sterically hindered groups.^{34,52,53}

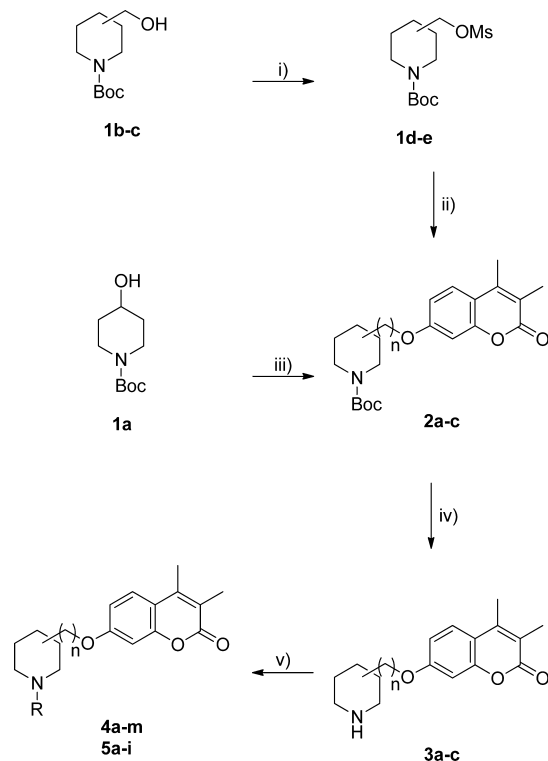
The designed compounds were tested in vitro to evaluate
their ability to inhibit both ChEs and MAOs. The ability of
novel compounds to permeate the blood–brain barrier (BBB)
was preliminarily calculated in silico by using Volsurf+ package
(Molecular Discovery, London, UK) to compute Log BB, a
molecular interaction field (MIF) based parameter useful to
estimate the CNS distribution of small molecules.⁵⁴ The most
promising compounds fished out from both the enzymatic
screening and in silico BBB-permeation prediction were
prioritized and studied in human SH-SY5Y neuroblastoma
cell lines for their cytotoxicity and potential neuroprotective
effects against oxidative insults (hydrogen peroxide, rotenone,
and oligomycin A). Moreover, compounds endowed with the

148 highest neuroprotective effects were evaluated in vitro for their
149 ability to cross BBB in a Madin–Darby canine kidney
150 (MDCKII-MDR1) cell model and to interact with glycoprotein-P
151 (P-gp) mediated transport. The hydrophilic/lipophilic
152 balance of selected compounds was investigated through well-
153 established turbidimetric determination of aqueous solubility
154 and RP-HPLC lipophilicity measurements.

155 CHEMISTRY

156 **Scheme 1** illustrates the synthetic pathway to piperidine
157 derivatives **4a–m** and (\pm)-**5a–i** reported in **Table 1**. The

Scheme 1. Synthesis of Compounds 4a–m, (\pm)-5a–i^a



^aReagents and conditions: (i) methanesulfonyl chloride, triethylamine, CH_2Cl_2 , 3 h, room temperature; (ii) 3,4-dimethyl-7-hydroxycoumarin, triethylamine, Cs_2CO_3 , dry DMF, 72 h, 70 °C; (iii) 3,4-dimethyl-7-hydroxycoumarin, ADDP, PPh_3 , triethylamine, anhydrous CH_2Cl_2 , 15 h, room temperature; (iv) trifluoroacetic acid, CH_2Cl_2 , 1 h, 0 °C to room temperature; (v) for **4a**, **4i**, and **5a**, methyl iodide, anhydrous K_2CO_3 , acetone, 6 h, room temperature; for **4b–h**, **4j–m**, and **5b–h**, butyl iodide (for **4b**) or substituted benzyl bromide, anhydrous K_2CO_3 , acetone, 30 min, 130 °C, MW; for **5i**, 3,4-dimethoxybenzaldehyde, sodium triacetoxyborohydride, 1,2-dichloroethane, 15 h, room temperature.

158 preparation of compounds bearing a methylene spacer started
159 from the activation of Boc-protected 3- and 4-piperidineme-
160 thanol **1b,c** as mesylate esters (**1d,e**) that underwent SN
161 3,4-dimethyl-7-hydroxycoumarin in DMF at 70 °C by using
162 cesium carbonate as the base and triethylamine to buffer the
163 reaction mixture, thus obtaining intermediates **2b,c**. Coumarins
164 lacking the methylene linker were synthesized starting from the
165 Mitsunobu etherification to couple **1a** with 3,4-dimethyl-7-
166 hydroxycoumarin⁵⁵ under buffered conditions through triethyl-
167 amine, thus yielding **2a**. The removal of the carbamate
168 protecting group of **2a–c** in acidic conditions by TFA
169 unmasked the piperidine intermediates **3a–c** that underwent

final alkylation under microwave-assisted nucleophilic sub-
stitution conditions (compounds **4b–h**, **4j–m**, (\pm)-**5a–i**) in
acetonitrile with the appropriate benzyl bromide or methylation
at room temperature (**4a**, **4i**, and (\pm)-**5a**). $\text{NaBH}(\text{OAc})_3$
mediated the reductive amination of **3c** and commercially
available 3,4-dimethoxybenzaldehyde to prepare coumarin
(\pm)-**5i**. A sequential two-step alkylation protocol under
microwave irradiation afforded the rigid 1,2,3,4-tetrahydroiso-
quinoline derivatives **7a,b** (**Scheme 2**). Initially, 3,4-dimethyl-7-
hydroxycoumarin was reacted with 1,3- or 1,4-dibromoalkane,
thus furnishing intermediate bromides **6a,b**. Under the same
reaction conditions, the suitable 1,2,3,4-tetrahydroisoquinoline
was alkylated with **6a,b**, yielding the desired compounds **7a,b**.

Biological Assays. All compounds were tested in vitro for
their inhibitory activities on human MAOs (hMAOs), electric
eel AChE (eeAChE), and equine serum BChE (esBChE)
enzymes. For hMAOs inhibition assay, the protocol was carried
out with a fluorescence-based method using kynuramine as a
nonselective substrate of hMAO A and hMAO B.^{34,56} As for
ChEs, the well-known Ellman's spectrophotometric test⁵⁷ was
used to determine IC_{50} s for both isoforms. The inhibition data
are reported in **Table 1** as IC_{50} (μM) or, for poorly active
compounds, as percentage of inhibition at 10 μM . The kinetic
behavior of compound (\pm)-**5b** for the inhibition of eeAChE
was investigated and is illustrated in **Figure 2** by means of a
Lineweaver–Burk diagram, where the reciprocals of enzyme
activity (eeAChE) vs reciprocals of substrate (S-acetylthiocho-
line) concentration in the presence of different concentrations
(0–8 μM) of inhibitor have been reported.

Human neuroblastoma SH-SY5Y cell lines were used to
evaluate the cytotoxic effect of compounds **4j–k**, (\pm)-**5a–e**,
and (\pm)-**5i** through the 3-(4,5-dimethylthiazol-2-yl)-2,5-diphe-
nyltetrazolium bromide (MTT) viability assay (**Figure 3**).⁵⁸ By
using the same cellular models,⁵⁹ the ability of selected
compounds to protect neurons against three different toxic
insults (hydrogen peroxide, oligomycin-A, and rotenone) was
studied (**Figure 4**) and compared to donepezil taken as a
reference anti-Alzheimer's drug. Data concerning cytotoxicity
and neuroprotection assays are expressed as percentage of
viability referred to control experiment as illustrated in **Figures**
3 and **4**.

As previously reported,³⁴ cell-based transport studies were
aimed at monitoring the BBB permeating potential of
compounds (\pm)-**5a,b** and (\pm)-**5d** displaying the highest
neuroprotective activity. Bidirectional transport studies were
carried out by measuring apical to basolateral (AP-BL) and
basolateral to apical (BL-AP) apparent permeability (P_{app}) in
MDCK cells. After retroviral transfection with the human
MDR1 cDNA (MDCKII-MDR1), these cells highly express P-
gp, thus alerting compounds likely to be efflux pumps
substrates. P_{app} (in units of cm/s) and efflux ratio (ER) were
calculated and summarized in **Table 2**.

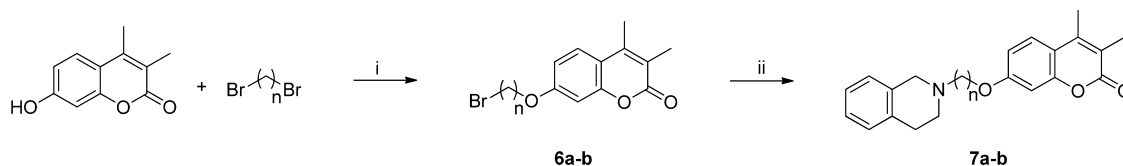
RESULTS AND DISCUSSION

It is worth underlining that MAO B selectivity of the
multipotent ligands reported herein was a pursued feature to
avoid well-known side effects raising from the inhibition of
peripheral MAO A isoform. On the other hand, isoform
selectivity was not considered a crucial issue in the case of
ChEs. In fact, in advanced AD increasing body of evidence
supports the importance of BChE whose activity increases as
the disease progresses. Both ChEs are capable of catalyzing the

Table 1. MAOs and ChEs Inhibition Data for Compounds 4a–m, (±)-5a–i, and 7a,b

compd	n	X	R	logBBB ^d	IC ₅₀ , μM (or inhibition % at 10 μM)			
					MAO A ^b	MAO B ^b	AChE ^c	BChE ^d
4a	0		H	0.586	11.7±3.1	0.274±0.053	1.30 ±0.12	11±1%
4b	0		<i>n</i> -Pr	0.707	23.9±2.0	1.409±0.452	0.99 ±0.17	35±3%
4c	0		Ph	0.609	3.59±0.17	0.445±0.049	0.78 ±0.11	9.57 ±0.18
4d	0		3-ClPh	0.530	0.87±0.45	0.285±0.026	1.08 ±0.06	28±2%
4e	0		4-ClPh	0.618	1.59±0.01	0.876±0.021	1.55 ±0.24	29±2%
4f	0		4-CNPh	0.235	1.29±0.39	0.656±0.144	0.97 ±0.16	48±1%
4g	0		Bn	0.717	12.4±0.1	2.49±0.38	1.65 ±0.49	1.77 ±0.37
4h	0		PhCO	0.425	1.96±0.13	0.114±0.020	3.78 ±0.52	45±3%
4i ^d	1		H	0.471	16.6±1.8	0.297±0.059	0.68 ±0.16	14±1%
4j ^d	1		Ph	0.547	2.41±1.51	0.105 ±0.001	1.66 ±0.42	4.72 ±0.71
4k ^d	1		3-ClPh	0.548	0.70±0.12	0.089±0.002	1.03 ±0.03	6.07 ±0.11
4l ^d	1		4-ClPh	0.569	37%	0.614±0.085	9.57 ±0.12	19±3%
4m ^d	1		4-CNPh	0.122	10.1±0.3	0.549±0.020	1.81 ±0.77	27±3%
(±)-5a ^d	1		H	0.551	9.33±0.21	0.137±0.022	0.80 ±0.08	19±1%
(±)-5b ^d	1		Ph	0.477	2.81±0.80	0.030±0.005	1.03 ±0.05	3.41±0.19
(+)-5b	1		Ph	0.477	3.84±0.15	0.023±0.003	1.80±0.29	2.91±0.03
(-)-5b	1		Ph	0.477	2.30±0.47	0.195±0.076	0.78±0.01	8.08±0.48
(±)-5c ^d	1		3-ClPh	0.457	0.98±0.08	0.036±0.014	1.17 ±0.45	4.69 ±0.39
(±)-5d ^d	1		3-BrPh	0.557	0.81±0.16	0.110±0.021	1.91 ±0.65	30±3%
(+)-5d	1		3-BrPh	0.557	0.54±0.20	0.026±0.005	3.23 ±0.23	36±1%
(-)-5d	1		3-BrPh	0.557	1.11±0.10	0.196±0.008	1.72 ±0.04	26±2%
(±)-5e ^d	1		4-FPh	0.494	1.11±0.27	0.163±0.002	1.46 ±0.45	3.69 ±0.31
(±)-5f ^d	1		4-ClPh	0.557	0.822±0.002	0.050±0.011	2.89 ±0.72	5.90 ±0.21
(±)-5g ^d	1		4-MeSO ₂ Ph	0.011	0.21±0.03	0.113±0.021	0.85 ±0.02	10±1%
(±)-5h ^d	1		4-CNPh	0.148	4.51±1.47	0.034±0.004	2.80 ±0.35	36±1%
(±)-5i	1		3,4-diMeOPh	0.306	1.72±0.06	0.090±0.006	2.21 ±0.52	6.04 ±0.25
7a ^d	3			0.451	2.68±0.85	0.298±0.003	1.22 ±0.13	0.95±0.10
7b ^d	4			0.476	2.24±0.28	0.612±0.040	1.15 ±0.01	2.61±0.25
donepezil							0.021 ±0.002	2.31±0.12
clorgyline					0.0025 ±0.0003	2.55±0.55		
pargyline					10.9±0.6	2.69±0.48		

^aCalculated with Volsurf+ package (Molecular Discovery, Perugia, Italy). ^bHuman recombinant MAOs on Supersomes. ^cAChE from Electric eel. ^dBChE from horse serum.

Scheme 2. Synthesis of Compounds 7a–b^a

^aReagents and conditions: (i) dibromoalkyl derivative, anhydrous K_2CO_3 , acetone, 130 °C, 30 min, MW; (ii) 1,2,3,4-tetrahydroisoquinoline, anhydrous K_2CO_3 , acetone, 130 °C, 30 min, MW.

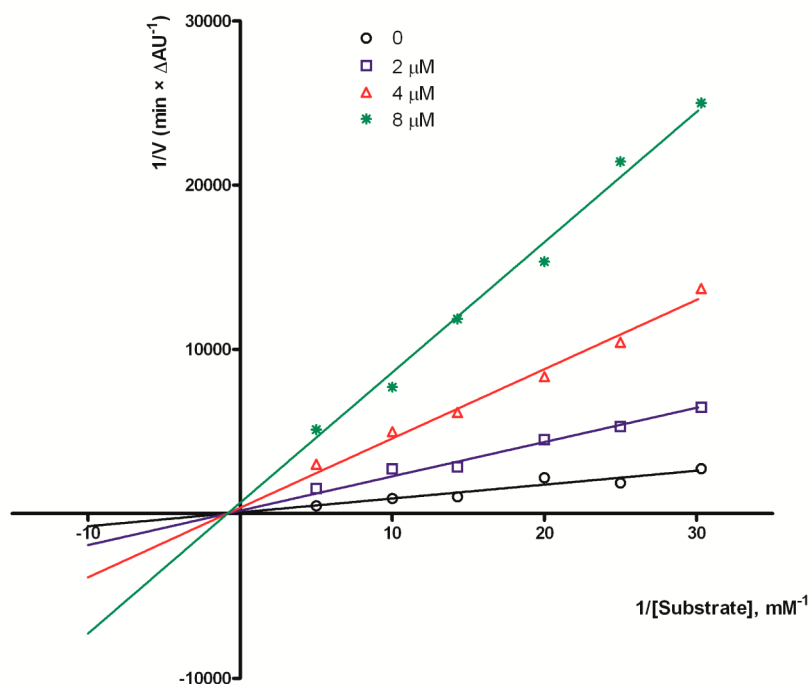


Figure 2. Lineweaver–Burk plots of *ee*ACHE inhibition kinetics of compound (\pm)-5b. Reciprocals of enzyme activity (*ee*AChE) vs reciprocals of substrate (*S*-acetylthiocholine) concentration in the presence of different concentrations (0–8 μ M) of inhibitor. Inset: Concentrations used for inhibitors are coded with different graphic symbols.

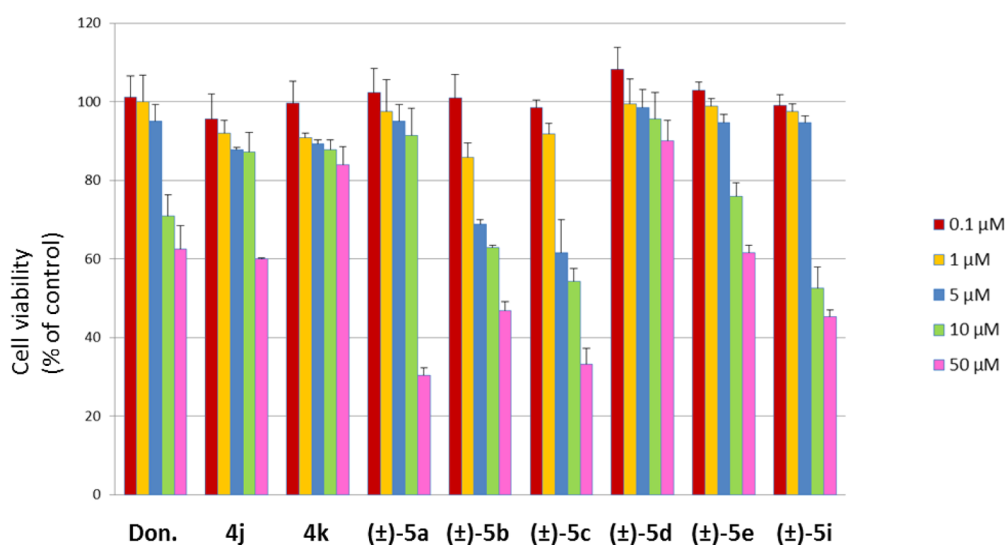


Figure 3. Cytotoxicity of compounds 4j–k, (\pm)-5a–e, and (\pm)-5i tested at concentrations in the range 0.1–50 μ M in human neuroblastoma SH-SY5Y cell lines for 24 h. Data are reported as percentage of cell survival vs untreated cells (control). Data represent means \pm SD ($n = 3$).

231 hydrolysis of ACh. Therefore, BChE inhibition can be a viable
232 strategy to counteract the cholinergic depletion too.²⁵

Keeping the 3,4-dimethylcoumarin as the common structural 233
feature, the main modifications regarded the flexibility and 234

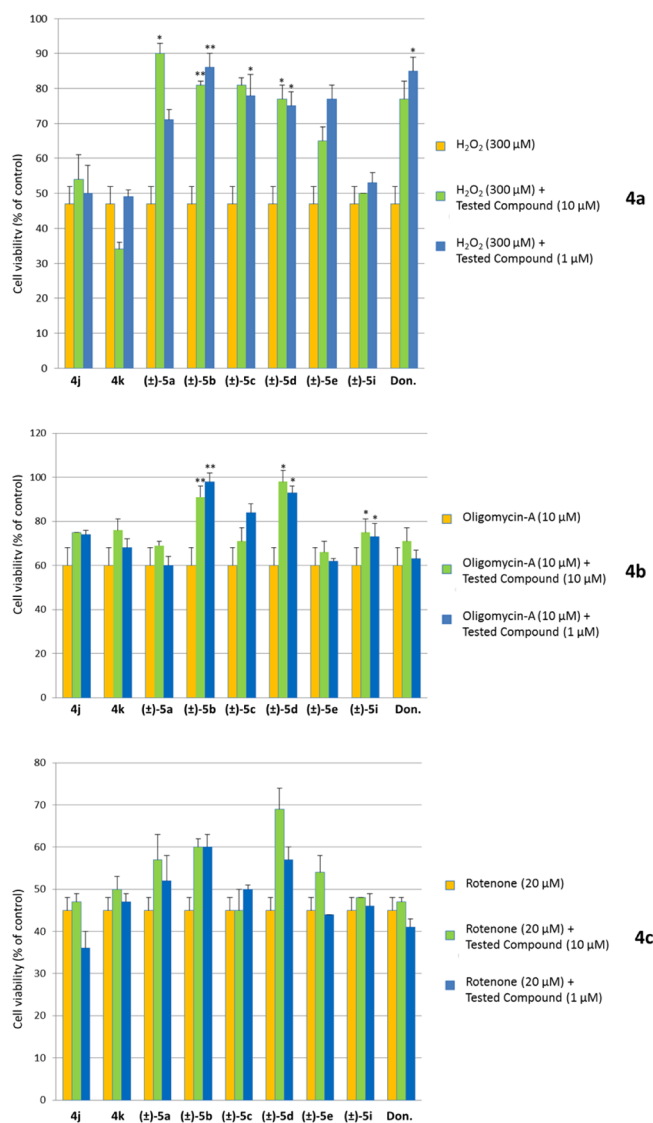


Figure 4. Neuroprotective effect on human neuroblastoma SH-SY5Y cells of selected compounds **4j–k**, **(±)-5a–e**, and **(±)-5i** after 24 h incubation at different concentrations (1 and 10 μM) with H_2O_2 (300 μM (**4a**)), oligomycin-A (10 μM (**4b**)), and rotenone (20 μM (**4c**)). Data are expressed as percentage of viable cells (referred to control) and shown as mean \pm SD ($n = 3$). Untreated cells were used as control. Donepezil was used as a reference anti-AD marketed drug. Statistical significance was calculated using a two-way analysis of variance (ANOVA) followed by the Bonferroni post-hoc tests (GraphPad Prism version 5); * $p < 0.05$, ** $p < 0.01$.

Table 2. Bidirectional Transport across MDCKII-MDR1 Cells of Compounds **(±)-5a,b** and **(±)-5d**

compd	P_{app} AP-BL (cm/s)	P_{app} BL-AP (cm/s)	ER ^a
(±)-5a	$2.23 \pm 0.11 \times 10^{-5}$	$2.02 \pm 0.7 \times 10^{-5}$	0.90
(±)-5b	$2.43 \pm 0.65 \times 10^{-5}$	$1.48 \pm 0.30 \times 10^{-5}$	0.61
(±)-5d	$8.40 \pm 0.25 \times 10^{-7}$	$2.16 \pm 0.22 \times 10^{-6}$	2.56
diazepam	$2.58 \pm 0.03 \times 10^{-5}$	$2.53 \pm 0.05 \times 10^{-5}$	0.98
FD-4	$8.94 \pm 0.15 \times 10^{-6}$	$8.03 \pm 0.20 \times 10^{-6}$	0.89

^aEfflux ratio (ER) was calculated using the following equation: $\text{ER} = P_{\text{app}} \text{ BL-AP} / P_{\text{app}} \text{ AP-BL}$, where $P_{\text{app}} \text{ BL-AP}$ is the apparent permeability of basal-to-apical transport, and $P_{\text{app}} \text{ AP-BL}$ is the apparent permeability of apical-to-basal transport. An efflux ratio greater than 2 indicates that a test compound is likely to be a substrate for P-gp transport.

more pronounced effect of the substitution pattern on the MAO affinity.

All hybrids displayed from moderate to high affinity toward hMAO B with submicromolar IC_{50} s but for **4b** and **4g**. All compounds inhibited selectively MAO B, with selectivity index (SI, $\text{IC}_{50} \text{ MAO A} / \text{IC}_{50} \text{ MAO B}$) ranging from 2 (**4e,f**) to 133 (**(±)-5h**).

Furthermore, MAO B affinity was affected by the flexibility of the linker and the piperidine substitution site (3 vs 4) more than AChE affinity. In fact, higher MAO B inhibitory potencies could be fished out from compounds **4i–m** and **(±)-5a–i**, where a methylene spacer tethers the basic head to the planar coumarin. In absence of the spacer, increasing the size and lipophilicity of the substituent on piperidine nitrogen from methyl (**4a**) to *n*-butyl (**4b**) and benzyl group (**4c**) decreased MAO B affinity while improving AChE affinity. The opposite trend was observed in the presence of the methylene linker connecting the coumarin to the 3- and 4-substituted piperidinyl ring when moving from methyl to benzyl (**4i** vs **4j**), **(±)-5a** vs **(±)-5b**). Homologation of the terminal chain from benzyl (**4c**) to phenethyl (**4g**) group influenced negatively the affinities toward both MAOs and reduced AChE affinity, too. The introduction of a carbonyl group (**4h**) produced a 4-fold MAO B affinity improvement with respect to **4c**, whereas AChE inhibitory potency diminished.

The substitution position at the piperidine cycle strongly influenced MAO B affinity. As a matter of fact, three derivatives out of the 4-substituted piperidine series (**4a–m**) showed an $\text{IC}_{50} < 0.250 \mu\text{M}$ whereas all 3-substituted piperidines **(±)-5a–i** showed MAO B inhibitory potencies $< 0.250 \mu\text{M}$. The presence of 3-substituted piperidines was preferred from MAO B with respect to 4-piperidinyl moieties (**(±)-5a** > **4a** and **4b**; **(±)-5b** > **4c** and **4j**; **(±)-5c** > **4d** and **4k**; **(±)-5f** > **4e** and **4l**; **(±)-5h** > **4f** and **4m**), irrespective of the nitrogen substituents. Looking at the basic head, the introduction of halogens (3'-Cl, 3'-Br, 4'-F, 4'-Cl) as well as electron-withdrawing (4'-SO₂CH₃ and 4'-CN) and electron-donating groups (3',4'-diOMe) on the phenyl ring exhibited a detrimental effect regards to MAO B affinity and drastically reduced MAO B/A selectivity. Meta-substitution represented the preferred position for chlorine in the binding to MAO B enzymatic cleft, as inferred by comparing **4d** vs **4e**, **4k** vs **4l**, and **(±)-5c** vs **(±)-5f**. In the *para* position, a cyano group was preferred to chloro (**4e** < **4f**, **4l** < **4m**), **(±)-5f** < **(±)-5h**) in both MAO B and AChE. Sulfonyl derivative **(±)-5g** displayed the highest MAO A affinity along with a low IC_{50} toward MAO B.

geometry of the linker tethering the coumarin backbone at position 7 to the basic head and the alkylation of the piperidine nitrogen.

Looking at the inhibition data for piperidine-bearing coumarins reported in Table 1, as expected from the presence of the *N*-benzylpiperidine moiety mimicking donepezil, all compounds showed from good to high affinity toward AChE (IC_{50} s $\leq 10 \mu\text{M}$) along with good selectivity values over BChE. AChE inhibitory potencies shift was not remarkably influenced by the structural modification herein reported and IC_{50} s for AChE laid in the range 0.68 μM (**4i**) –9.57 μM (**4l**). In contrast, a wider activity window could be observed for MAO B (0.030 μM for **(±)-5b** < IC_{50} s < 2.49 μM for **4g**), suggesting a

To assess the AChE inhibition mechanism of donepezil-like *N*-benzyl-piperidines, the kinetic behavior of compound (\pm)-**5b** was investigated. As shown in Figure 2, Lineweaver–Burk plot indicated a mixed-type inhibition with a K_i equal to $1.37 \pm 0.05 \mu\text{M}$, thus suggesting a partial occupancy of PAS and potential $\text{A}\beta$ antiaggregating properties.

HPLC separations were undertaken to check a possible influence of chirality in the binding interactions of this series, and racemic mixtures of **5b** and **5d** were resolved as prototypes on a CHIRALPAK IA column, yielding enantiomeric excess $>99\%$ (see Supporting Information for details). Regarding hMAO B affinity, an eudismic ratio equal to 8 was observed for both racemates. Eutomers (+)-**5b** and (+)-**5d** exhibited outstanding hMAO B affinities ($\text{IC}_{50} = 23$ and 26 nM , respectively). Interestingly, the most potent enantiomer (+)-**5b** showed also an outstanding MAO B over MAO A selectivity ($\text{SI} = 167$), much greater than the other eutomer (+)-**5d** ($\text{SI} = 21$). Both mixtures displayed a lower activity ratio (≤ 2) toward hMAO A, being (+)-**5b** and (–)-**5d** the distomers. A lower and inverted eudismic ratio was found toward eeAChE for both pairs of enantiomers.

To overcome the undesirable drawback of chirality, 1,2,3,4-tetrahydroisoquinoline derivatives **7a,b** were designed as rigid achiral analogues of the most potent hit compound ((\pm)-**5b**). In vitro evaluation proved a sharp drop of MAO B affinity, albeit the potency was still in the nanomolar range. Interestingly, compounds **7a,b** showed low micromolar affinities toward both ChEs, with **7a** being the most potent BChE inhibitor of the whole series with a submicromolar $\text{IC}_{50} = 0.95 \mu\text{M}$. This result could be ascribed to the flatness and wideness of BChE enzymatic cleft that could better accommodate rigid and sterically hindered basic groups.

To assess the brain-permeating capability of the novel multipotent molecules reported herein, Volsurf+ was employed to compute Log BB, a parameter expressing the logarithmic ratio between the concentration of a drug in brain and blood. More specifically, compounds showing Log BB value greater than 0.5 readily penetrate into CNS and are classified as BBB+. Log BB values lower than -0.5 disclose very poor brain permeation (BBB– compounds), whereas values higher than -0.5 and lower than 0.5 indicate moderate permeation (BBB \pm compounds).⁶⁰ Calculations suggested that most compounds in Table 1 should rapidly be distributed into the brain (BBB+ compounds). Log BB of derivatives bearing polar substituents on the phenyl ring (a cyano-group for **4f**, **4m**, and (\pm)-**5h** or a dimethoxy-group for (\pm)-**5i**) and the keto-derivative **4h** suggested moderate permeation. The lowest Log BB value (0.011) was returned by (\pm)-**5g** with a highly hydrophilic substituent on the basic head ($-\text{SO}_2\text{CH}_3$ group). The high confidence of Volsurf-based predictions was assessed through the projection of the studied compounds in the chemical space represented by its applicability domain, determined according to the Hotelling's T-squared approach (see Supporting Information).⁶¹

Cell-Based Assays: Cytotoxicity, Neuroprotection, and Brain Permeation. By combining data from enzymatic screening with in silico calculations, a number of hits was shortlisted and selected for further assays in cell-based models in order to evaluate their cytotoxic and neuroprotective effects and their ability to permeate BBB without interacting with efflux pumps such as P-gp. Regarding the inhibitory properties, the following selection criteria were applied: (i) IC_{50} toward MAO B $< 150 \text{ nM}$, (ii) IC_{50} toward AChE $< 2 \mu\text{M}$. With

respect to brain permeation predictions, Log BB threshold was set equal to 0.450. Seven coumarin derivatives (**4j**, **4k**, (\pm)-**5a**, (\pm)-**5b**, (\pm)-**5c**, (\pm)-**5d**, and (\pm)-**5e**) met all the selection criteria and were submitted to preliminary in vitro investigations in human neuroblastoma SH-SY5Y cell lines. Compound (\pm)-**5i** was also included in the study in order to investigate the effect of the *ortho*-dimethoxyphenyl moiety.

Because in vitro enzymatic assays for both enantiomers of **5b** and **5d** provided AChE inhibition activities close to racemate and the differences between enantiomers and racemate for MAO B were reasonably low (ratio of $\text{IC}_{50}\text{s} < 6$ for both isomers in comparison to racemate **5b** and **5d**), we deemed unnecessary to perform the cell-based studies on single enantiomers at this early stage of investigations.

As shown in Figure 3, most compounds displayed negligible cytotoxicity up to $50 \mu\text{M}$ after 24 h incubations. Some derivatives produced a reasonable cellular damage only at highest concentrations. In particular, the concentrations responsible for 50% inhibition of cell growth (IC_{50}s) for compounds (\pm)-**5a**, (\pm)-**5b**, (\pm)-**5c**, and (\pm)-**5i** were equal to 30 ± 0.01 , 44 ± 0.02 , 13 ± 0.01 , and $10 \pm 0.03 \mu\text{M}$, respectively.

The overproduction of harmful radicals, above all reactive oxygenated species (ROS), and the unbalance in detoxification systems produces severe oxidative stress conditions in neurons affected by AD. Nucleic acids, proteins, and lipids become loaded with aberrant alterations that, in turn, could trigger AD-related neurotoxicity, and indeed the reduction of oxidative stress has been claimed as a viable strategy to slow down the progression of the disease. Therefore, we tested also the ability of selected multitarget molecules to protect SH-SY5Y cells against oxidative injuries. The cytoprotective effect was determined by measuring cell viability after incubation with a radical initiator (hydrogen peroxide, H_2O_2) and two mitochondrial poisons (rotenone and oligomycin-A), both capable of arresting respiratory chain and energy production (Figure 4). Rotenone induces cellular damage by interfering with the activity of complex I of the respiratory chain,⁶² whereas oligomycin-A binds to F_0 part of H^+ -ATP-synthase⁶³ and exerts its pro-apoptotic effect by blocking ATP formation. Compounds under investigation were incubated at two concentrations (1 and $10 \mu\text{M}$), and untreated cells were used as control. As depicted in Figure 4a, compounds (\pm)-**5a–e** markedly protected SH-SY5Y cells against H_2O_2 even at the lowest concentration ($1 \mu\text{M}$). A low increase of cell viability in the presence of oligomycin-A was produced by **4j** (at 1 and $10 \mu\text{M}$), **4k** (at $1 \mu\text{M}$), (\pm)-**5c** (at $10 \mu\text{M}$), and (\pm)-**5i** (at 1 and $10 \mu\text{M}$). Moreover, derivative (\pm)-**5a** was not able to counteract cellular damage induced by oligomycin-A, whereas it exerted a moderate neuroprotective activity against rotenone at 1 and $10 \mu\text{M}$. A significant increase of viable cells was obtained when rotenone was coincubated with (\pm)-**5e** at $1 \mu\text{M}$. Derivative (\pm)-**5b** and (\pm)-**5d** remarkably increased cell viability in the presence of both mitochondrial toxins used in this assay (rotenone and oligomycin-A) at 1 and $10 \mu\text{M}$ and exerted a cytoprotective activity by far superior to that of donepezil. Taken together, these results highlighted dual inhibitors (\pm)-**5b** and (\pm)-**5d** as the most promising neuroprotective agents of the series as they proved to be effective against all the insults employed in SH-SY5Y cell-based experimental models.

To endorse the potential of both compounds as promising multipotent anti-AD leads, in vitro transport studies were

undertaken. As for CNS-acting drugs, a critical issue represented by the ability to cross the BBB, acting as a highly lipophilic boundary.⁶⁴ Compounds permeate BBB mainly by a passive diffusion mechanism, and several efflux systems prevent the entrance of xenobiotics into CNS. Because the extrusion activity is essentially governed by P-gp, the possible behavior of a hit as a P-gp substrate should be assessed in the early stage of drug discovery along with its brain permeation properties. MDCK cells were used as a model to examine the behavior of selected compounds in crossing the BBB and eventually interacting with extrusion pumps. When retrovirally transfected with the human MDR1 cDNA (MDCKII-MDR1), these cell lines highly express P-gp (MDR1) and represent a robust BBB mimicking in vitro model. Furthermore, permeation analyses were undertaken also with (\pm)-**5a**, being the most potent neuroprotective agent against H₂O₂ at 10 μ M and moderately effective against rotenone at both tested concentrations (1 and 10 μ M). In contrast with the computed Log BB, lipophilic derivative (\pm)-**5d** was not able to permeate the monolayer (see Table 2), probably because of quite high membrane retention as deduced from low permeation rate in both directions, i.e., apical-to-basolateral (AP-BL) and basolateral-to-apical (BL-AP). Moreover, an ER > 2 (ER = P_{app} BL-AP/ P_{app} AP-BL) can be taken as a figure of undesirable interactions with P-gp. On the other hand, as shown in Table 2 compounds (\pm)-**5b** and (\pm)-**5a** confirmed rapid permeation and low ER comparable to donepezil used as reference CNS-active drug, thus envisaging good brain distribution and poor interactions as P-gp substrates.

Aqueous Solubility and Lipophilicity. In the present work, the aim of optimizing the aqueous solubility at pH 7.4 of a coumarin-based hit recently reported by us (7-(4-(*N*-benzyl-*N*-methylaminomethyl)benzyloxy)-4-(hydroxymethyl)-2*H*-chromen-2-one hydrochloride **I**,³⁴ Figure 1) while maintaining a dual AChE-MAO B inhibitory activity was pursued by introducing focused structural modification on the protonatable head and on the linker at position 7 of the coumarin core. Kinetic aqueous solubility at pH 7.4 was experimentally determined for compounds **I**, **4j**, **5a**, and **5b** by applying a turbidimetric method.

As showed in Table 3, compound **I** returned the lowest value of water solubility ($\log S = -4.42$) and the *N*-methylpiperidin-3-yl derivative **5a** exhibited the highest solubility ($\log S = -3.67$). Compared to **I**, the piperidin-4-yl derivative **4j** showed only a modest increase of solubility ($\log S = -4.25$), whereas the isomer piperidin-3-yl derivative **5b** proved to be 3-fold more soluble (119 μ M, $\log S = -3.92$).

Table 3. Aqueous Solubility and Lipophilicity Index of Compounds **I,³⁴ **4j**, (\pm)-**5a**, and (\pm)-**5b****

compd	$\log S$ (pH 7.4) ^a	$\log k'$ ^b	cLogP ^c
I ³⁴	-4.42 \pm 0.09	1.87	4.08
4j	-4.25 \pm 0.08	1.98	5.16
(\pm)- 5a	-3.67 \pm 0.07	1.14	3.79
(\pm)- 5b	-3.92 \pm 0.05	2.01	5.55

^a $\log S$ (mol/L). Measured at pH 7.40 in 50 mM Tris-HCl, pH 7.4, at room temperature. Data are the mean \pm SEM of three independent assays. ^bExtrapolated value at 65% of ammonium acetate buffer (pH 5.00) from six measurements. Mobile phase: methanol/ammonium acetate buffer (pH 5.00, 20 mM) v/v from 70% to 45%. Data are the mean \pm SEM of three independent assays. ^cBio-Loom version 1.6, Biobyte Corp., Claremont, USA.

The observed increase in water solubility at pH 7.4 of **4j**, **5a**, and **5b** over **I**, and the small but significant differences among them as well, could be reasonably explained taking into account the pK_a shift (i.e., the degree of amine protonation) in the examined molecules and their hydrophobicity. Regarding the basicity of the amino moiety at C(7) of the coumarin core, the ACD/laboratories (version 6.00) software estimates pK_as of 7.8 for **I**, about 8.5 for **4j** and **5b**, and about 9.4 for **5a** (all values are however within the optimal range 7.5–10.5 proposed for CNS drugs).⁶⁵ The lipophilicity of the molecules in neutral form was assessed by calculation (Bio-Loom 1.6, Biobyte Corp., Claremont, USA), whereas a relative lipophilicity scale of the compounds, predominantly in the protonated form, was experimentally determined by a reversed phase (RP) HPLC method. Zorbax Eclipse-C18 column was used as the stationary phase, and mixtures of ammonium acetate buffer (20 mM, pH 5.00) and methanol were used as the mobile phases to measure chromatographic capacity factor ($\log k'$) as a lipophilicity index.

Looking at the data in Table 3, interesting structure–property relations could be derived. Quite obviously, the most water-soluble is **5a**, that is, the most hydrophilic one (i.e., the lowest $\log k'$ and cLogP values) and fully protonated at pH 7.4. Both *N*-benzylpiperidinyl derivatives **4j** and **5b**, despite their higher lipophilicity (as supported by the cLogP and $\log k'$ values), are more soluble in water than **I**, most likely due to the different protonation degree of the amino group which, based on the estimated pK_as, should be higher in **4j** and **5b** than in **I**. Albeit showing similar lipophilicity and very close basicity, the piperidin-3-yl derivative **5b** proved to be more than 2-fold more soluble in water than the isomer piperidin-4-yl compound **4j**. This result may be related on one hand to the disruption of molecular symmetry elements in **5b** with respect to **4j**, which could be an entropic factor favoring solubility in water, whereas on the other hand, the proximity of the polar groups in **5b**, which are closer than in **4j**, could explain the slightly better partitioning of **5b** in apolar media, as cLogP and $\log k'$ values account for.

CONCLUSIONS

The multitarget approach has been extensively exploited by several research groups as a promising therapeutic option to face neurodegenerative disorders.^{66–69} In the case of AD, in the last decades inhibition of enzymatic activities of MAOs and ChEs has been pursued to identifying novel therapeutic agents with a potential disease-modifying effect.^{70,71} A seminal discovery in the field is represented by ladostigil,⁷² a dual AChE-MAO inhibitor⁷³ that has been recently announced to finish ad interim phase IIb and to enter phase III clinical trials by Avraham Pharmaceuticals for the treatment of mild cognitive impairment.⁷⁴ Looking at the literature, common drawbacks of multitarget dual inhibitors hitting MAOs and ChEs are given by low MAO B over MAO A selectivity and, at least, one violation of Lipinski's Rule of Five (in most cases MW > 500 and/or cLogP > 5), the latter representing a compromising feature for good oral bioavailability. Peripheral inhibition of MAO A implies safety issues arising from the so-called cheese effect.⁷⁵ Over the years, we devoted attention to the development of coumarin-based dual AChE-MAO B inhibitors. To this end, our design strategy was aimed at improving the physicochemical properties for drug bioavailability (aqueous solubility, above all) of a previously described multipotent hit compound³⁴ while maintaining a dual AChE-MAO B inhibitory activity. Such a compound (i.e., derivative **I**

529 in ref 34, Figure 1) showed outstanding in vitro inhibitory
530 potencies against hAChE and hMAO B in the nanomolar range
531 along with a limited aqueous solubility at pH 7.4 (38 μM).

532 Structure–activity relationships (SARs) of multipotent
533 compounds described herein shed light on the most relevant
534 structural features modulating hMAO B affinity: (i) the
535 flexibility of the spacer linking the coumarin core to the basic
536 tail at position 7 and (ii) the substituents and the branching
537 position on the piperidinyl ring (1,3 vs 1,4). AChE affinity was
538 influenced by these structural modifications to a lesser extent.
539 Interestingly, the presence of piperidinyl fragment along with
540 its substitution pattern markedly influenced aqueous solubility.

541 The present study allowed the development of a novel
542 multifunctional agent (\pm)-**5b** with a good balance of
543 biochemical activities and improved aqueous solubility,
544 definitively deserving further attention. In vitro enzymatic
545 assays highlighted an outstanding hMAO B affinity (IC_{50} = 30
546 nM) along with pronounced MAO B/A selectivity (SI = 94)
547 and low micromolar eeAChE affinity (IC_{50} = 1.03 μM). In cell-
548 based assays, (\pm)-**5b** produced low cytotoxic damage (IC_{50} =
549 $44 \pm 0.02 \mu\text{M}$) after 24 h incubation and increased cell viability
550 of human neuroblastoma lines incubated with some toxic
551 insults (H_2O_2 , rotenone, and oligomycin-A). Interestingly, its
552 neuroprotective activity against the oxidative stress insults
553 produced by hydrogen peroxide, oligomycin-A, and rotenone
554 was superior to that of donepezil, used as a reference anti-AD
555 drug. Bidirectional transport studies on MDCKII-MDR1 model
556 denoted a rapid BBB permeation without suffering from likely
557 P-gp interactions, thus suggesting good brain permeation and
558 CNS distribution. Moreover, coumarin (\pm)-**5b** does not violate
559 Lipinski's Rule of Five (MW = 377.48, HB-donor = 0–1
560 depending on the protonation state, HB-acceptor = 2–3
561 depending on the protonation form, cLogP (ChemAxon) =
562 4.57). The presence of the basic piperidinyl moiety does
563 increase water solubility of **5b** at pH 7.4 (3-fold increase
564 compared to **1**³⁴). Taken together, these findings highlighted
565 the potential of this class of compounds and particularly of
566 (\pm)-**5b** as multitarget anti-AD neurotherapeutic, deserving
567 further pharmacological investigations to prove its ability to
568 prevent the onset, hamper the progression, or reverse the
569 neurodegenerative process in animal models.

570 ■ EXPERIMENTAL SECTION

571 **Chemistry.** Starting materials, reagents, intermediate **1a**, and
572 analytical grade solvents were purchased from Sigma-Aldrich
573 (Europe). The purity of all the intermediates, checked by ^1H NMR
574 and HPLC, was always better than 95%. All the newly prepared and
575 tested compounds showed HPLC purity higher than 98%. Column
576 chromatography was performed using Merck silica gel 60 (0.063–
577 0.200 mm, 70–230 mesh). Flash chromatographic separations were
578 performed on a Biotage SP1 purification system using flash cartridges
579 prepacked with KP-Sil 32–63 μm , 60 Å silica. All reactions were
580 routinely checked by TLC using Merck Kieselgel 60 F_{254} aluminum
581 plates and visualized by UV light or iodine. Regarding the reaction
582 requiring the use of dry solvents, the glassware was flame-dried and
583 then cooled under a stream of dry argon before use. Optical rotation
584 was measured on a PerkinElmer 241 polarimeter with a Na lamp (589
585 nm). Nuclear magnetic resonance spectra were recorded on a Varian
586 Mercury 300 instrument (at 300 MHz) or on an Agilent Technologies
587 500 apparatus (at 500 MHz) at ambient temperature in the specified
588 deuterated solvent. Chemical shifts (δ) are quoted in parts per million
589 (ppm) and are referenced to the residual solvent peak. The coupling
590 constants J are given in hertz (Hz). The following abbreviations were
591 used: s (singlet), d (doublet), dd (doublet of doublet), t (triplet), q
592 (quadruplet), qn (quintuplet), m (multiplet), br s (broad signal);

signals due to OH and NH protons were located by deuterium 593
exchange with D_2O . Chiral HPLC separations and enantiomeric excess 594
determinations were carried out on CHIRALPAK IA (Chiral 595
Technologies Europe, 25 cm \times 0.46 cm I.D., 5 μm size particles) 596
built on a Analytic Agilent 1260 Infinity multidetector system 597
equipped with 1200 series UV-diode array in isocratic conditions. 598
Elemental analyses were performed on the EuroEA 3000 analyzer only 599
on the final compounds tested as MAOs and ChEs inhibitors. The 600
measured values for C, H, and N agreed to within $\pm 0.40\%$ of the 601
theoretical values. Melting points were determined by the capillary 602
method on a Stuart Scientific SMP3 electrothermal apparatus and are 603
uncorrected. 604

General Procedure for the Synthesis of tert-Butyl 3- and 4- 605
Hydroxymethylpiperidine-1-carboxylate (1b–c). To a suspension of 606
the suitable commercially available 3- and 4-hydroxymethylpiperidine 607
(8.6 g, 75 mmol) in a mixture of acetonitrile (110 mL) and saturated 608
aq sodium hydrogen carbonate solution (35 mL), di-tert-butyl 609
dicarbonate (21 g, 94 mmol) was added in portions while cooling 610
to 0 °C. The reaction mixture was then kept to room temperature and 611
left under magnetic stirring for 18 h. Brine (300 mL) was added, and 612
the aqueous layer was extracted with ethyl acetate (3 \times 150 mL). The 613
organic phases were collected, dried over sodium sulfate, and 614
evaporated to dryness to give the desired product that was used 615
without further purification. 616

tert-Butyl 4-(Hydroxymethyl)piperidine-1-carboxylate (1b). Yield: 617
88%. ^1H NMR (300 MHz, CDCl_3) δ : 1.06–1.19 (m, 2H), 1.44 (s, 618
9H), 1.60–1.74 (m, 4H), 2.69 (t, J = 12.7 Hz, 2H), 3.48 (t, J = 5.8 Hz, 619
2H), 4.09–4.13 (m, 2H, 1H dis. with D_2O). 620

tert-Butyl 3-(Hydroxymethyl)piperidine-1-carboxylate (1c). Yield: 621
94%. ^1H NMR (500 MHz, $\text{DMSO}-d_6$) δ : 1.01–1.10 (m, 1H), 1.21– 622
1.47 (m, 3H), 1.37 (s, 9H), 1.52–1.68 (m, 2H), 2.63–2.72 (m, 1H), 623
3.11–3.19 (m, 1H), 3.21–3.28 (m, 1H), 3.73–3.81 (m, 1H), 3.87– 624
3.96 (m, 1H), 4.48 (t, J = 8.8 Hz, 1H, dis. with D_2O). 625

General Procedure for the Synthesis of tert-Butyl 4- 626
[[[(Methylsulfonyl)oxy]methyl]piperidine-1-carboxylate (1d) and 627
tert-Butyl 3-[[[(Methylsulfonyl)oxy]methyl]piperidine-1-carboxylate 628
(1e). The suitable Boc-protected piperidine **1b,c** (7.5 g, 35 629
mmol) was dissolved in CH_2Cl_2 (100 mL) before the addition of 630
triethylamine (20 mL, 140 mmol). The mixture was cooled to 0 °C 631
with an external ice bath, and methanesulfonyl chloride (3.0 mL, 39 632
mmol) was added dropwise. After warming at room temperature, the 633
reaction was kept under magnetic stirring for 3 h. The mixture was 634
diluted with CH_2Cl_2 (200 mL) and washed with satd aq Na_2CO_3 (3 \times 635
200 mL). The organic phase was dried over Na_2SO_4 . Evaporation of 636
the solvent yielded the desired product in high purity. 637

tert-Butyl 4-[[[(Methylsulfonyl)oxy]methyl]piperidine-1-carboxy- 638
late (1d). Yield: 86%. ^1H NMR (500 MHz, $\text{DMSO}-d_6$) δ : 1.03– 639
1.11 (m, 2H), 1.38 (s, 9H), 1.61–1.65 (m, 2H), 1.82–1.88 (m, 1H), 640
2.62–2.75 (br s, 2H), 3.15 (s, 3H), 3.90–3.97 (m, 2H), 4.04 (d, J = 641
6.4 Hz, 2H). 642

tert-Butyl 3-[[[(Methylsulfonyl)oxy]methyl]piperidine-1-carboxy- 643
late (1e). Yield: 85%. ^1H NMR (500 MHz, $\text{DMSO}-d_6$) δ : 1.20–1.26 644
(m, 1H), 1.28–1.35 (m, 1H), 1.38 (s, 9H), 1.56–1.62 (m, 1H), 1.69– 645
1.74 (m, 1H), 1.76–1.82 (m, 1H), 2.78–2.84 (m, 2H), 3.16 (s, 3H), 646
3.67–3.72 (br s, 2H), 4.01–4.10 (m, 2H). 647

tert-Butyl 4-[(3,4-Dimethyl-2-oxo-2H-chromen-7-yl)oxy]- 648
piperidine-1-carboxylate (2a). Triethylamine (17 mL, 120 mmol), 649
commercially available **1a** (8.1 g, 40 mmol), and 1,1'-(azodicarbonyl)- 650
dipiperidine (20 g, 80 mmol) were added to a suspension of 3,4- 651
dimethyl-7-hydroxycoumarin (15 g, 80 mmol) in dry CH_2Cl_2 (250 652
mL). The reaction mixture was kept to 0 °C and triphenylphosphine 653
(21 g, 80 mmol), previously dissolved in CH_2Cl_2 (100 mL), was added 654
dropwise. The reaction was kept to room temperature and left under 655
magnetic stirring overnight. The solvent was evaporated under 656
reduced pressure, and the resulting crude solid was purified through 657
flash chromatography (gradient eluent: ethyl acetate in *n*-hexane 20% 658
 \rightarrow 60%). Yield: 60%. ^1H NMR (300 MHz, CDCl_3) δ : 1.47 (s, 9H), 659
1.71–1.82 (m, 2H), 1.92–1.98 (m, 2H), 2.18 (s, 3H), 2.37 (s, 3H), 660
3.31–3.39 (m, 2H), 3.66–3.74 (m, 2H), 4.48–4.55 (m, 1H), 6.80 (d, J 661

662 = 2.2 Hz, 1H), 6.84 (dd, $J_1 = 2.2$ Hz, $J_2 = 8.8$ Hz, 1H), 7.50 (d, $J = 8.8$ Hz, 1H).

664 **General Procedure for the Synthesis of tert-Butyl 3- or 4-((3,4-Dimethyl-2-oxo-2H-chromen-7-yl)oxy)methyl)piperidine-1-carboxylate (2b,c).** The appropriate mesylate ester **1d,e** (8.2 g, 28 mmol) was dissolved in dry DMF (50 mL) followed by the addition of triethylamine (7.8 g, 56 mmol), cesium carbonate (9.1 g, 28 mmol), and 3,4-dimethyl-7-hydroxycoumarin (4.5 g, 28 mmol). After heating at 70 °C for 72 h, the mixture was poured onto crushed ice (500 g). The precipitate was collected and thoroughly washed with water, thus furnishing the desired derivative **2b,c**.

673 **tert-Butyl 4-((3,4-Dimethyl-2-oxo-2H-chromen-7-yl)oxy)methyl)piperidine-1-carboxylate (2b).** Yield: 85%. ¹H NMR (300 MHz, CDCl₃) δ: 1.24–1.33 (m, 2H), 1.46 (s, 9H), 1.77–1.86 (m, 2H), 1.93–2.03 (m, 1H), 2.18 (s, 3H), 2.37 (s, 3H), 2.75 (t, $J = 12.4$ Hz, 2H), 3.84–3.86 (m, 2H), 4.16–4.18 (m, 2H), 6.77 (d, $J = 2.5$ Hz, 1H), 6.83 (dd, $J_1 = 2.5$ Hz, $J_2 = 8.8$ Hz, 1H), 7.49 (d, $J = 8.8$ Hz, 1H).

679 **tert-Butyl 3-((3,4-Dimethyl-2-oxo-2H-chromen-7-yl)oxy)methyl)piperidine-1-carboxylate (2c).** Yield: 89%. ¹H NMR (300 MHz, DMSO-*d*₆) δ: 1.33 (s, 9H), 1.26–1.35 (m, 2H), 1.59–1.66 (m, 1H), 1.71–1.83 (m, 1H), 1.85–1.91 (m, 1H), 2.00 (s, 3H), 2.35 (s, 3H), 2.80–2.95 (m, 2H), 3.88–3.97 (m, 4H), 6.91–6.95 (m, 2H), 7.68 (d, $J = 8.8$ Hz, 1H).

685 **General Procedure for the Synthesis of 3,4-Dimethyl-7-(piperidin-4-yloxy)-2H-chromen-2-one (3a) and 3,4-Dimethyl-7-(piperidin-3- and 4-ylmethoxy)-2H-chromen-2-one (3b,c).** To a solution of **2a** (7.5 g, 20 mmol) or **2b,c** (7.7 g, 20 mmol) in CH₂Cl₂ (40 mL), 689 trifluoroacetic acid (40 mL) was added dropwise while cooling to 0 °C. After 15 min, the reaction mixture was kept to room temperature and left under magnetic stirring for 1 h. The solvents and excess trifluoroacetic acid were removed under reduced pressure. The resulting oil was diluted with ethyl acetate (100 mL) and washed with Na₂CO₃ (3 × 30 mL). The organic phase was dried over Na₂SO₄ and concentrated to dryness, thus obtaining the unprotected piperidines as white solids.

697 **3,4-Dimethyl-7-(piperidin-4-yloxy)-2H-chromen-2-one (3a).** Yield: 83%. ¹H NMR (500 MHz, DMSO-*d*₆) δ: 1.77–1.84 (m, 2H), 2.06 (s, 3H), 2.08–2.15 (m, 2H), 2.35 (s, 3H), 3.06–3.12 (m, 2H), 3.22–3.31 (m, 2H), 4.73–4.78 (m, 1H), 6.96–6.98 (m, 1H), 7.07–7.08 (m, 1H), 7.68–7.70 (m, 1H), NH not detected.

702 **3,4-Dimethyl-7-(piperidin-4-ylmethoxy)-2H-chromen-2-one (3b).** Yield: 89%. ¹H NMR (300 MHz, DMSO-*d*₆) δ: 1.38–1.51 (m, 2H), 1.86–1.95 (m, 2H), 2.03–2.11 (m, 5H), 2.35 (s, 3H), 2.84–2.98 (m, 2H), 3.25–3.34 (m, 2H), 3.95–3.97 (m, 2H), 6.91 (d, $J = 2.5$ Hz, 1H), 6.94 (dd, $J_1 = 2.5$ Hz, $J_2 = 8.8$ Hz, 1H), 7.68 (d, $J = 8.8$ Hz, 1H).

707 **3,4-Dimethyl-7-(piperidin-3-ylmethoxy)-2H-chromen-2-one (3c).** Yield: 92%. ¹H NMR (300 MHz, DMSO-*d*₆) δ: 1.21–1.38 (m, 2H), 1.58–1.64 (m, 1H), 1.80–1.84 (m, 2H), 2.05 (s, 3H), 2.19 (br s, 1H), 2.34 (s, 3H), 2.73–2.81 (m, 2H), 3.22–3.37 (m, 2H), 3.92–4.05 (m, 2H), 6.91–6.95 (m, 2H), 7.69 (d, $J = 8.3$ Hz, 1H).

712 **General Procedure for the Synthesis of Final Compounds 4a, 4i, and 5a.** The appropriate coumarin **3a–c** (0.50 mmol) was suspended in dry acetone (5 mL) before the addition of potassium carbonate (0.069 g, 0.50 mmol) and methyl iodide (0.031 mL, 0.50 mmol). The mixture was stirred at room temperature for 6 h. The inorganic residue was then filtered off, and the resulting solution was concentrated to dryness under rotary evaporation. The desired products were purified as described below.

720 **3,4-Dimethyl-7-[(N-methylpiperidin-4-yl)oxy]-2H-chromen-2-one (4a).** Purification procedure: the crude was treated with THF, and the insoluble residue was filtered off. Evaporation of the solvent under rotary evaporation and crystallization from *n*-hexane furnished the desired product. Yield: 59%; mp 95–96 °C (*n*-hexane). ¹H NMR (300 MHz, CDCl₃) δ: 1.88–1.96 (m, 2H), 2.10–2.15 (m, 2H), 2.18 (s, 2H), 2.37 (s, 3H), 2.38 (s, 3H), 2.40–2.50 (m, 2H), 2.75–2.80 (m, 2H), 4.41 (br s, 1H), 6.80 (d, $J = 2.5$ Hz, 1H), 6.84 (dd, $J_1 = 2.5$ Hz, $J_2 = 8.8$ Hz, 1H), 7.49 (d, $J = 8.8$ Hz, 1H). Anal. (C₁₇H₂₁NO₃) Calcd %: C, 71.06; H, 7.37; N, 4.87. Found %: C, 71.39; H, 7.23; N, 5.02.

730 **3,4-Dimethyl-7-[(N-methylpiperidin-4-yl)methoxy]-2H-chromen-2-one Hydrochloride (4i).** Purification procedure: the crude was treated with HCl 1.25 N in ethanol, collecting the precipitate. Yield:

65%; mp > 250 °C. ¹H NMR (300 MHz, DMSO-*d*₆) δ: 1.57–1.65 (m, 2H), 1.91–1.96 (m, 3H), 2.05 (s, 3H), 2.35 (s, 3H), 2.68 (s, 3H), 2.89–2.99 (m, 2H), 3.36–3.42 (m, 2H), 3.94 (d, $J = 6.0$ Hz, 2H), 6.91–6.97 (m, 2H), 7.69 (d, $J = 9.0$ Hz, 1H), 10.40 (br s, 1H, dis. with D₂O). Anal. (C₁₈H₂₃NO₃·HCl) Calcd %: C, 63.99; H, 7.16; N, 4.15. Found %: C, 64.31; H, 7.26; N, 4.20.

738 **(±)-3,4-Dimethyl-7-[(N-methylpiperidin-3-yl)methoxy]-2H-chromen-2-one Hydrochloride (5a).** Purification procedure: the crude was treated with HCl 1.25 N in ethanol, yielding a precipitate that was collected and washed with ethanol. Yield: 60%; mp 150–152 °C. ¹H NMR (300 MHz, DMSO-*d*₆) δ: 1.19–1.30 (m, 1H), 1.70–1.89 (m, 4H), 2.06 (s, 3H), 2.35 (s, 3H), 2.76 (s, 3H), 3.25–3.54 (m, 4H), 3.89–4.08 (m, 2H), 6.91–6.97 (m, 2H), 7.70 (d, $J = 9.0$ Hz, 1H), 9.91 (br s, 1H, dis. with D₂O). Anal. (C₁₈H₂₃NO₃·HCl) Calcd %: C, 63.99; H, 7.16; N, 4.15. Found %: C, 63.89; H, 7.21; N, 3.93.

742 **General Procedure for the Synthesis of Final Compounds 4b–h, 4j–m, and (±)-5b–h.** A Pyrex vessel was charged with a magnetic stirring and a Weflon bar, and then the appropriate 3,4-dimethyl-7-(piperidin-3- and 4-yloxy)-2H-chromen-2-one **3a,b**, or 3,4-dimethyl-7-(piperidin-3- and 4-ylmethoxy)-2H-chromen-2-one **3c,d** derivative (0.50 mmol) and potassium carbonate (1.0 mmol) were suspended in acetone (4.0 mL). The suitable commercially available butyl chloride (0.50 mmol, for **4b**) or substituted benzyl bromide (0.5 mmol) was added. The reactor was placed in a microwave apparatus and irradiated at 130 °C for 30 min. After cooling to room temperature, the solid residue was filtered off after thorough washing with CH₂Cl₂. The solution was concentrated to dryness, and the resulting crude was purified as detailed below. Compounds **4j–m**, **(±)-5b–h**, **7a,b** were obtained as hydrochloride salts as described below.

751 **3,4-Dimethyl-7-[(N-butylpiperidin-4-yl)oxy]-2H-chromen-2-one (4b).** Isolation procedure: column chromatography (eluent: methanol in chloroform 5%) followed by crystallization from hot ethanol. Yield: 55%; mp 86–87 °C (ethanol). ¹H NMR (300 MHz, CDCl₃) δ: 0.98 (t, $J = 7.3$ Hz, 3H), 1.39–1.46 (m, 2H), 1.91–1.98 (m, 2H), 2.18–2.23 (m, 2H), 2.20 (s, 3H), 2.38 (s, 3H), 2.76–2.83 (m, 2H), 2.93–3.04 (m, 2H), 3.06–3.12 (m, 2H), 3.42–3.46 (m, 2H), 4.76–4.79 (m, 1H), 6.81–6.85 (m, 2H), 7.54 (d, $J = 8.5$ Hz, 1H). Anal. (C₂₀H₂₇NO₃) Calcd %: C, 72.92; H, 8.26; N, 4.25. Found %: C, 73.34; H, 8.10; N, 3.97.

762 **3,4-Dimethyl-7-[(N-benzylpiperidin-4-yl)oxy]-2H-chromen-2-one (4c).** Isolation procedure: crystallization from hot ethanol. Yield: 82%; mp 111–112 °C (ethanol). ¹H NMR (300 MHz, CDCl₃) δ: 1.89–2.07 (m, 4H), 2.19 (s, 3H), 2.32–2.38 (m, 5H), 2.77–2.85 (m, 2H), 3.51–3.57 (m, 2H), 4.37–4.45 (m, 1H), 6.77–6.90 (m, 2H), 7.24–7.34 (m, 5H), 7.49 (d, $J = 8.5$ Hz, 1H). Anal. (C₂₃H₂₅NO₃) Calcd %: C, 76.00; H, 6.93; N, 3.85. Found %: C, 76.01; H, 6.89; N, 4.01.

773 **3,4-Dimethyl-7-[(N-(3-chlorobenzyl)piperidin-4-yl)oxy]-2H-chromen-2-one (4d).** Isolation procedure: crystallization from hot ethanol. Yield: 84%; mp 106–107 °C (ethanol). ¹H NMR (300 MHz, CDCl₃) δ: 1.83–1.91 (m, 2H), 2.02–2.07 (m, 2H), 2.18 (s, 3H), 2.34–2.40 (m, 5H), 2.70–2.77 (m, 2H), 3.51–3.56 (m, 2H), 4.37–4.43 (m, 1H), 6.80 (d, $J = 2.5$ Hz, 1H), 6.83 (dd, $J_1 = 2.5$ Hz, $J_2 = 8.5$ Hz, 1H), 7.23–7.29 (m, 3H), 7.37 (s, 1H), 7.49 (d, $J = 8.5$ Hz, 1H). Anal. (C₂₃H₂₄ClNO₃) Calcd %: C, 69.43; H, 6.08; N, 3.52. Found %: C, 69.70; H, 6.06; N, 3.56.

781 **3,4-Dimethyl-7-[(N-(4-chlorobenzyl)piperidin-4-yl)oxy]-2H-chromen-2-one (4e).** Isolation procedure: crystallization from hot ethanol. Yield: 87%; mp 140–141 °C (ethanol). ¹H NMR (300 MHz, CDCl₃) δ: 1.83–1.89 (m, 2H), 1.98–2.05 (m, 2H), 2.18 (s, 3H), 2.27–2.33 (m, 2H), 2.36 (s, 3H), 2.70–2.77 (m, 2H), 3.52 (s, 2H), 4.36–4.41 (m, 1H), 6.79 (d, $J = 2.5$ Hz, 1H), 6.83 (dd, $J_1 = 2.5$ Hz, $J_2 = 8.5$ Hz, 1H), 7.28–7.33 (m, 4H), 7.48 (d, $J = 8.5$ Hz, 1H). Anal. (C₂₃H₂₄ClNO₃) Calcd %: C, 69.43; H, 6.08; N, 3.52. Found %: C, 69.43; H, 6.13; N, 3.85.

792 **4-[(4-((3,4-Dimethyl-2-oxochromen-7-yl)oxy)piperidin-1-yl)methyl]benzonitrile (4f).** Isolation procedure: crystallization from hot ethanol. Yield: 71%; mp 120–121 °C (ethanol). ¹H NMR (300 MHz, CDCl₃) δ: 1.79–2.00 (m, 4H), 2.18 (s, 3H), 2.35–2.38 (m, 5H), 2.78–2.82 (m, 2H), 3.50–3.56 (m, 2H), 4.41 (s, 1H), 6.79 (d, $J = 2.5$ Hz, 1H), 6.82 (dd, $J_1 = 2.5$ Hz, $J_2 = 8.8$ Hz, 1H), 7.15–7.33 (m, 4H), 802

803 7.49 (d, $J = 8.8$ Hz, 1H). Anal. ($C_{24}H_{24}N_2O_3$) Calcd %: C, 74.21; H, 804 6.23; N, 7.21. Found %: C, 74.74; H, 6.19; N, 7.21.

805 **3,4-Dimethyl-7-[(N-(2-phenylethyl)piperidin-4-yl)oxy]-2H-chro-**
806 **men-2-one (4g)**. Isolation procedure: crystallization from hot ethanol.
807 Yield: 87%; mp 107–108 °C (ethanol). 1H NMR (300 MHz, $CDCl_3$)
808 δ : 1.93–2.01 (m, 2H), 2.17–2.20 (m, 4H), 2.35–2.39 (m, 4H), 2.72–
809 2.95 (m, 8H), 4.45–4.51 (m, 1H), 6.81 (d, $J = 2.5$ Hz, 1H), 6.84 (dd,
810 $J_1 = 2.5$ Hz, $J_2 = 8.5$ Hz, 1H), 7.22–7.33 (m, 5H), 7.50 (d, $J = 8.5$ Hz,
811 1H). Anal. ($C_{24}H_{27}NO_3$) Calcd %: C, 76.36; H, 7.21; N, 3.71. Found
812 %: C, 76.53; H, 7.14; N, 3.97.

813 **3,4-Dimethyl-7-[(N-(2-phenyl-2-oxoethyl)piperidin-4-yl)oxy]-2H-**
814 **chromen-2-one (4h)**. Isolation procedure: crystallization from hot
815 ethanol. Yield: 90%; mp 94–96 °C (dec) from ethanol. 1H NMR (300
816 MHz, $CDCl_3$) δ : 1.63–1.72 (m, 2H), 2.05–2.16 (m, 2H), 2.19 (s,
817 3H), 2.34–2.41 (m, 5H), 2.96–3.02 (m, 2H), 4.19–4.27 (m, 2H),
818 4.57–4.63 (m, 1H), 6.85 (d, $J = 2.5$ Hz, 1H), 6.89 (dd, $J_1 = 2.5$ Hz, J_2
819 = 8.8 Hz, 1H), 7.51 (t, $J = 7.1$ Hz, 2H), 7.52 (d, $J = 8.8$ Hz, 1H), 7.64
820 (t, $J = 7.1$ Hz, 1H), 7.98 (d, $J = 7.1$ Hz, 2H). Anal. ($C_{24}H_{25}NO_4$) Calcd
821 %: C, 73.64; H, 6.44; N, 3.58. Found %: C, 74.15; H, 6.38; N, 3.85.

822 **3,4-Dimethyl-7-[(N-benzylpiperidin-4-yl)methoxy]-2H-chromen-**
823 **2-one Hydrochloride (4j)**. Isolation procedure: column chromatog-
824 raphy (eluent: ethyl acetate in chloroform 50%). The compound was
825 transformed into the corresponding hydrochloride salt by dissolving
826 the solid free base in the minimum volume of 1,4-dioxane before
827 adding HCl 4.0 N in 1,4-dioxane. The resulting precipitate was
828 collected by filtration and washed with dry dioxane, yielding **4j**. Yield:
829 60%; mp 215–216 °C (dec). 1H NMR (300 MHz, $DMSO-d_6$) δ :
830 1.87–1.95 (m, 2H), 2.06 (s, 3H), 2.22–2.29 (m, 3H), 2.35 (s, 3H),
831 2.79–2.84 (m, 2H), 3.13–3.20 (m, 2H), 3.91–4.03 (m, 2H), 4.31–
832 4.35 (m, 2H), 6.88–6.96 (m, 2H), 7.46–7.58 (m, 5H), 7.69 (d, $J = 9.1$
833 Hz, 1H), 9.68 (s, 1H, dis. with D_2O). Anal. ($C_{24}H_{27}NO_3 \cdot HCl$) Calcd
834 %: C, 69.64; H, 6.82; N, 3.38. Found %: C, 70.09; H, 6.55; N, 3.40.

835 **3,4-Dimethyl-7-[(N-(3-chlorobenzyl)piperidin-4-yl)methoxy]-2H-**
836 **chromen-2-one Hydrochloride (4k)**. Isolation procedure: the crude
837 was suspended in 1,4-dioxane and the insoluble residue discarded. HCl
838 4.0 N in 1,4-dioxane was added to the solution, yielding a white
839 precipitate that was filtered and crystallized from hot ethanol. Yield:
840 99%; mp 246–248 °C (ethanol). 1H NMR (300 MHz, $DMSO-d_6$) δ :
841 1.55–1.66 (m, 2H), 1.90–1.97 (m, 3H), 2.06 (s, 3H), 2.35 (s, 3H),
842 2.89–3.00 (m, 2H), 3.35–3.42 (m, 2H), 3.94 (d, $J = 6.0$ Hz, 2H),
843 4.26–4.30 (m, 2H), 6.91 (dd, $J_1 = 2.5$ Hz, $J_2 = 8.8$ Hz, 1H), 6.95 (d, J
844 = 2.5 Hz, 1H), 7.48–7.55 (m, 3H), 7.66–7.71 (m, 2H), 10.16 (s, 1H,
845 dis. with D_2O). Anal. ($C_{24}H_{26}ClNO_3 \cdot HCl$) Calcd %: C, 64.29; H,
846 6.07; N, 3.12. Found %: C, 64.68; H, 5.88; N, 2.83.

847 **3,4-Dimethyl-7-[(N-(4-chlorobenzyl)piperidin-4-yl)methoxy]-2H-**
848 **chromen-2-one Hydrochloride (4l)**. Isolation procedure: the crude
849 was suspended in 1,4-dioxane and the insoluble residue was discarded
850 after filtration. HCl 4.0 N in 1,4-dioxane was added to the solution,
851 yielding a white precipitate that was filtered and crystallized from hot
852 ethanol. Yield: 77%; mp > 250 °C (ethanol). 1H NMR (300 MHz,
853 $DMSO-d_6$) δ : 1.57–1.65 (m, 2H), 1.92–1.97 (m, 3H), 2.05 (s, 3H),
854 2.35 (s, 3H), 2.91–2.99 (m, 2H), 3.38–3.45 (m, 2H), 3.94 (d, $J = 6.0$
855 Hz, 2H), 4.25–4.28 (m, 2H), 6.91 (dd, $J_1 = 2.5$ Hz, $J_2 = 8.5$ Hz, 1H),
856 6.95 (d, $J = 2.5$ Hz, 1H), 7.53 (d, $J = 8.8$ Hz, 2H), 7.58 (d, $J = 8.8$ Hz,
857 2H), 7.67 (d, $J = 8.5$ Hz, 1H), 10.12 (s, 1H, dis. with D_2O). Anal.
858 ($C_{24}H_{26}ClNO_3 \cdot HCl$) Calcd %: C, 64.29; H, 6.07; N, 3.12. Found %:
859 C, 64.70; H, 6.00; N, 3.05.

860 **4-[[4-[(3,4-Dimethyl-2H-2-oxochromen-7-yl)oxymethyl]piperidin-**
861 **1-yl]methyl]benzonitrile Hydrochloride (4m)**. Isolation procedure:
862 the crude was suspended in 1,4-dioxane and the insoluble residue was
863 filtered off. HCl 4.0 N in 1,4-dioxane was added to the solution,
864 yielding a white precipitate that was filtered and crystallized from hot
865 ethanol. Yield: 93%; mp > 250 °C (ethanol). 1H NMR (300 MHz,
866 $DMSO-d_6$) δ : 1.64–1.79 (m, 2H), 1.88–1.97 (m, 3H), 2.05 (s, 3H),
867 2.34 (s, 3H), 2.94 (q, $J = 12.0$ Hz, 2H), 3.36–3.43 (m, 2H), 3.93 (d, J
868 = 6.3 Hz, 2H), 4.32–4.37 (m, 2H), 6.90–6.99 (m, 2H), 7.68 (d, $J =$
869 8.5 Hz, 1H), 7.86 (d, $J = 8.4$ Hz, 2H), 7.94 (d, $J = 8.4$ Hz, 2H), 11.17
870 (s, 1H, dis. with D_2O). Anal. ($C_{25}H_{26}N_2O_3 \cdot HCl$) Calcd %: C, 68.41;
871 H, 6.20; N, 6.38. Found %: C, 68.86; H, 6.03; N, 6.17.

(\pm)-**3,4-Dimethyl-7-[(N-benzylpiperidin-3-yl)methoxy]-2H-chro-**
872 **men-2-one Hydrochloride (5b)**. Isolation procedure: column
873 chromatography (eluent: ethyl acetate in chloroform 50%). The
874 compound was transformed into the corresponding hydrochloride salt
875 by dissolving the solid free base in the minimum volume of 1,4-
876 dioxane before adding HCl 4.0 N in 1,4-dioxane. The resulting
877 precipitate was collected by filtration and washed with dry dioxane,
878 yielding **5b**. Yield: 62%; mp 215–216 °C (dec). 1H NMR (300 MHz,
879 $DMSO-d_6$) δ : 1.20–1.34 (m, 1H), 1.60–1.75 (m, 1H), 1.77–1.90 (m,
880 2H), 2.06 (s, 3H), 2.20–2.27 (m, 1H), 2.35 (s, 3H), 2.72–2.86 (m,
881 2H), 3.30–3.49 (m, 2H), 3.90–4.07 (m, 2H), 4.28–4.33 (m, 2H),
882 6.90 (dd, $J_1 = 2.5$ Hz, $J_2 = 8.8$ Hz, 1H), 6.93 (d, $J = 2.5$ Hz, 1H), 7.42–
883 7.57 (m, 5H), 7.69 (d, $J = 8.8$ Hz, 1H), 10.12 (br s, 1H, dis. with
884 D_2O). Anal. ($C_{24}H_{27}NO_3 \cdot HCl$) Calcd %: C, 69.64; H, 6.82; N, 3.38.
885 Found %: C, 69.90; H, 6.81; N, 3.56.

(+)-**3,4-Dimethyl-7-[(N-benzylpiperidin-3-yl)methoxy]-2H-chro-**
887 **men-2-one (5b)**. HPLC purification of (\pm)-**5b** on a CHIRALPAK IA,
888 mobile phase, A = methanol, B = acetonitrile; isocratic elution, 20% B;
889 flow rate = 1 mL/min; $\lambda = 320$ nm; 100 μ L injection; k_2 . Melting
890 point: 117–119 °C. 1H NMR (500 MHz, $DMSO-d_6$) δ : 1.09–1.15
891 (m, 1H), 1.43–1.51 (m, 1H), 1.61–1.66 (m, 1H), 1.71–1.75 (m, 1H),
892 1.86–2.02 (m, 3H), 2.05 (s, 3H), 2.34 (s, 3H), 2.62–2.67 (m, 1H),
893 2.81–2.85 (m, 1H), 3.41 (d, $J = 13.7$ Hz, 1H), 3.47 (d, $J = 13.7$ Hz,
894 1H), 3.92 (d, $J = 6.4$ Hz, 2H), 6.87–6.90 (m, 2H), 7.19–7.23 (m,
895 1H), 7.25–7.30 (m, 4H), 7.65 (d, $J = 8.8$ Hz, 1H). $[\alpha]_D^{20} = +18.5^\circ$ (c
896 0.13, MeOH). Anal. ($C_{24}H_{27}NO_3$) Calcd %: C, 76.36; H, 7.21; N,
897 3.71. Found %: C, 76.50; H, 7.05; N, 3.46.

(-)-**3,4-Dimethyl-7-[(N-benzylpiperidin-3-yl)methoxy]-2H-chro-**
899 **men-2-one (5b)**. HPLC purification of (\pm)-**5b** on a CHIRALPAK IA,
900 mobile phase, A = methanol, B = acetonitrile; isocratic elution, 20% B;
901 flow rate = 1 mL/min; $\lambda = 320$ nm; 100 μ L injection; k_1 . Melting
902 point: 117–119 °C. 1H NMR (500 MHz, $DMSO-d_6$) δ : 1.07–1.14
903 (m, 1H), 1.42–1.51 (m, 1H), 1.61–1.66 (m, 1H), 1.70–1.78 (m, 1H),
904 1.84–2.02 (m, 3H), 2.05 (s, 3H), 2.34 (s, 3H), 2.62–2.67 (m, 1H),
905 2.81–2.85 (m, 1H), 3.42 (d, $J = 13.7$ Hz, 1H), 3.47 (d, $J = 13.7$ Hz,
906 1H), 3.91 (d, $J = 6.4$ Hz, 2H), 6.87–6.90 (m, 2H), 7.18–7.23 (m,
907 1H), 7.26–7.30 (m, 4H), 7.64 (d, $J = 8.8$ Hz, 1H). $[\alpha]_D^{20} = -18.5^\circ$ (c
908 0.13, MeOH). Anal. ($C_{24}H_{27}NO_3$) Calcd %: C, 76.36; H, 7.21; N,
909 3.71. Found %: C, 76.80; H, 6.91; N, 3.55.

(\pm)-**3,4-Dimethyl-7-[(N-(3-chlorobenzyl)piperidin-3-yl)methoxy]-**
911 **2H-chromen-2-one Hydrochloride (5c)**. Isolation procedure: the
912 crude was suspended in 1,4-dioxane and the insoluble residue was
913 filtered off. HCl 4.0 N in 1,4-dioxane was added to the solution,
914 yielding a white precipitate that was filtered and crystallized from hot
915 ethanol. Yield: 98%; mp 246–248 °C (dec) from ethanol. 1H NMR
916 (300 MHz, $DMSO-d_6$) δ : 1.21–1.35 (m, 1H), 1.77–1.85 (m, 3H),
917 2.05 (s, 3H), 2.34 (s, 3H), 2.36–2.43 (m, 1H), 2.81 (qn, $J = 11.5$ Hz,
918 2H), 3.37–3.48 (m, 2H), 3.94–4.06 (m, 2H), 4.32 (br s, 2H), 6.85–
919 6.93 (m, 2H), 7.45–7.54 (m, 3H), 7.45–7.70 (m, 2H), 10.30 (br s,
920 1H, dis. with D_2O). Anal. ($C_{24}H_{26}ClNO_3 \cdot HCl$) Calcd %: C, 64.29; H,
921 6.07; N, 3.12. Found %: C, 63.82; H, 5.85; N, 2.93.

(\pm)-**7-[[1-(3-Bromobenzyl)piperidin-3-yl]methoxy]-3,4-dimethyl-**
923 **2H-chromen-2-one Hydrochloride (5d)**. Isolation procedure: flash
924 chromatography (gradient eluent: ethyl acetate in *n*-hexane 20% \rightarrow
925 80%). The compound was transformed into the corresponding
926 hydrochloride salt by dissolving the solid free base in the minimum
927 volume of 1,4-dioxane before adding HCl 4.0 N in 1,4-dioxane. The
928 resulting precipitate was collected by filtration and washed with dry
929 dioxane, yielding racemic **5d**. Yield: 87%; mp 231–232 °C. 1H NMR
930 (free base, 300 MHz, $DMSO-d_6$) δ : 1.05–1.18 (m, 1H), 1.46–1.53
931 (m, 1H), 1.62–1.75 (m, 2H), 1.89–1.97 (m, 3H), 2.05 (s, 3H), 2.34
932 (s, 3H), 2.61–2.65 (m, 1H), 2.79–2.82 (m, 1H), 3.39–3.51 (m, 2H),
933 3.94 (d, $J = 6.1$ Hz, 2H), 6.86–6.89 (m, 2H), 7.21–7.29 (m, 2H),
934 7.40–7.45 (m, 2H), 7.65 (d, $J = 9.6$ Hz, 1H). Anal. ($C_{24}H_{26}BrNO_3 \cdot$
935 HCl) Calcd %: C, 58.49; H, 5.52; N, 2.84. Found %: C, 58.14; H, 5.48;
936 N, 2.98.

(+)-**7-[[1-(3-Bromobenzyl)piperidin-3-yl]methoxy]-3,4-dimethyl-**
938 **2H-chromen-2-one (5d)**. HPLC purification of (\pm)-**5d** on a
939 CHIRALPAK IA, mobile phase, A = methanol, B = acetonitrile;
940 isocratic elution, 30% B; flow rate = 1 mL/min; $\lambda = 320$ nm; 100 μ L
941

942 injection; k_2 . Melting point: 119–120 °C. ^1H NMR (300 MHz,
943 DMSO- d_6) δ : 1.03–1.18 (m, 1H), 1.46–1.53 (m, 1H), 1.64–1.75 (m,
944 2H), 1.87–1.97 (m, 3H), 2.05 (s, 3H), 2.34 (s, 3H), 2.60–2.65 (m,
945 1H), 2.79–2.82 (m, 1H), 3.39–3.51 (m, 2H), 3.93 (d, J = 6.1 Hz,
946 2H), 6.86–6.89 (m, 2H), 7.22–7.29 (m, 2H), 7.40–7.45 (m, 2H),
947 7.65 (d, J = 9.6 Hz, 1H). $[\alpha]_D^{20} = +33.5^\circ$ (c 0.08, MeOH). Anal.
948 ($\text{C}_{24}\text{H}_{26}\text{BrNO}_3$) Calcd %: C, 63.16; H, 5.74; N, 3.07. Found %: C,
949 63.50; H, 5.58; N, 3.00.

950 (–)-7-[[1-(3-Bromobenzyl)piperidin-3-yl]methoxy]-3,4-dimethyl-
951 2H-chromen-2-one (**5d**). HPLC purification of (\pm)-**5d** on a
952 CHIRALPAK IA, mobile phase, A = methanol, B = acetonitrile;
953 isocratic elution, 30% B; flow rate = 1 mL/min; λ = 320 nm; 100 μL
954 injection; k_1 . Melting point: 119–120 °C. ^1H NMR (300 MHz,
955 DMSO- d_6) δ : 1.05–1.18 (m, 1H), 1.46–1.53 (m, 1H), 1.62–1.75 (m,
956 2H), 1.89–1.97 (m, 3H), 2.07 (s, 3H), 2.33 (s, 3H), 2.61–2.67 (m,
957 1H), 2.80–2.84 (m, 1H), 3.36–3.51 (m, 2H), 3.94 (d, J = 6.1 Hz,
958 2H), 6.86–6.89 (m, 2H), 7.21–7.29 (m, 2H), 7.44–7.49 (m, 2H),
959 7.64 (d, J = 9.6 Hz, 1H). $[\alpha]_D^{20} = -33.5^\circ$ (c 0.08, MeOH). Anal.
960 ($\text{C}_{24}\text{H}_{26}\text{BrNO}_3$) Calcd %: C, 63.16; H, 5.74; N, 3.07. Found %: C,
961 63.49; H, 5.36; N, 2.96.

962 (\pm)-3,4-Dimethyl-7-[(N-(4-fluorobenzyl)piperidin-3-yl)methoxy]-
963 2H-chromen-2-one Hydrochloride (**5e**). Isolation procedure: the
964 crude was suspended in 1,4-dioxane and the insoluble residue was
965 filtered off. HCl 4.0 N in 1,4-dioxane was added to the solution,
966 yielding a white precipitate that was filtered and crystallized from hot
967 ethanol. Yield: 98%; mp 228–230 °C (dec). ^1H NMR (300 MHz,
968 DMSO- d_6) δ : 1.18–1.33 (m, 1H), 1.77–1.88 (m, 3H), 2.05 (s, 3H),
969 2.34 (s, 3H), 2.36–2.41 (m, 1H), 2.78 (qn, J = 9.9 Hz, 2H), 3.40–3.46
970 (m, 2H), 3.90–4.05 (m, 2H), 4.27–4.32 (m, 2H), 6.89 (dd, J_1 = 8.8
971 Hz, J_2 = 2.5 Hz, 1H), 6.93 (d, J = 2.5 Hz, 1H), 7.26–7.32 (m, 2H),
972 7.59–7.64 (m, 2H), 7.68 (d, J = 8.8 Hz, 1H), 10.34 (br s, 1H, dis. with
973 D_2O). Anal. ($\text{C}_{24}\text{H}_{26}\text{FNO}_3\cdot\text{HCl}$) Calcd %: C, 66.74; H, 6.30; N, 3.24.
974 Found %: C, 66.34; H, 6.22; N, 3.17.

975 (\pm)-3,4-Dimethyl-7-[(N-(4-chlorobenzyl)piperidin-3-yl)methoxy]-
976 2H-chromen-2-one Hydrochloride (**5f**). Isolation procedure: the
977 crude was suspended in 1,4-dioxane and the insoluble residue was
978 filtered off. HCl 4.0 N in 1,4-dioxane was added to the solution,
979 yielding a white precipitate that was filtered and crystallized from hot
980 ethanol. Yield: 91%; mp 219–221 °C (dec) from ethanol. ^1H NMR
981 (300 MHz, DMSO- d_6) δ : 1.18–1.34 (m, 1H), 1.76–1.88 (m, 3H),
982 2.05 (s, 3H), 2.35 (s, 3H), 2.36–2.41 (m, 1H), 2.71–2.86 (m, 2H),
983 3.39–3.46 (m, 2H), 3.90–4.05 (m, 2H), 4.29–4.31 (m, 2H), 6.88 (d, J
984 = 2.5 Hz, 1H), 6.93 (dd, J_1 = 2.5 Hz, J_2 = 8.8 Hz, 1H), 7.53 (d, J = 8.5
985 Hz, 2H), 7.59 (d, J = 8.5 Hz, 2H), 7.68 (d, J = 8.8 Hz, 1H), 10.37 (br
986 s, 1H, dis. with D_2O). Anal. ($\text{C}_{24}\text{H}_{26}\text{ClNO}_3\cdot\text{HCl}$) Calcd %: C, 64.29;
987 H, 6.07; N, 3.12. Found %: C, 63.86; H, 5.97; N, 3.09.

988 (\pm)-3,4-Dimethyl-7-[(N-(4-(methylsulfonyl)benzyl)piperidin-3-yl)-
989 methoxy]-2H-chromen-2-one Hydrochloride (**5g**). Isolation proce-
990 dure: the crude was suspended in 1,4-dioxane and the insoluble
991 residue was filtered off. HCl 4.0 N in 1,4-dioxane was added to the
992 solution, yielding a white precipitate that was filtered and crystallized
993 from hot ethanol. Yield: 99%; mp 172–174 °C (ethanol). ^1H NMR
994 (300 MHz, DMSO- d_6) δ : 1.20–1.36 (m, 1H), 1.80–1.87 (m, 3H),
995 2.05 (s, 3H), 2.34 (s, 3H), 2.40–2.46 (m, 1H), 2.76–2.87 (m, 2H),
996 3.24 (s, 3H), 3.28–3.48 (m, 2H), 3.91–4.03 (m, 2H), 4.40–4.45 (m,
997 2H), 6.89 (dd, J_1 = 2.5 Hz, J_2 = 8.8 Hz, 1H), 6.93 (d, J = 2.5 Hz, 1H),
998 7.68 (d, J = 8.8 Hz, 1H), 7.89 (d, J = 8.7 Hz, 2H), 8.00 (d, J = 8.7 Hz,
999 2H), 10.91 (br s, 1H, dis. with D_2O). Anal. ($\text{C}_{25}\text{H}_{29}\text{NO}_5\cdot\text{HCl}$) Calcd
1000 %: C, 61.03; H, 6.15; N, 2.85. Found %: C, 60.65; H, 5.84; N, 2.91.

1001 (\pm)-4-[(3-(3,4-Dimethyl-2H-2-oxochromen-7-yl)oxymethyl)-
1002 piperidin-1-yl]methyl]benzotrile Hydrochloride (**5h**). Isolation
1003 procedure: the crude was suspended in 1,4-dioxane and the insoluble
1004 residue was filtered off. HCl 4.0 N in 1,4-dioxane was added to the
1005 solution, yielding a white precipitate that was filtered and crystallized
1006 from hot ethanol. Yield: 76%; mp 220–222 °C (ethanol). ^1H NMR
1007 (300 MHz, DMSO- d_6) δ : 1.26–1.30 (m, 1H), 1.80–1.85 (m, 3H),
1008 2.06 (s, 3H), 2.35 (s, 3H), 2.39–2.43 (m, 1H), 2.76–2.87 (m, 2H),
1009 3.30–3.31 (m, 1H), 3.44–3.48 (m, 1H), 3.91–4.05 (m, 2H), 4.37–
1010 4.44 (m, 2H), 6.88–6.94 (m, 2H), 7.69 (d, J = 8.7 Hz, 1H), 7.77 (d, J
1011 = 7.8 Hz, 2H), 7.95 (d, J = 7.8 Hz, 2H), 10.30 (br s, 1H, dis. with

D_2O). Anal. ($\text{C}_{25}\text{H}_{26}\text{N}_2\text{O}_3\cdot\text{HCl}$) Calcd %: C, 68.41; H, 6.20; N, 6.38.
1012 Found %: C, 68.77; H, 6.05; N, 6.17.

1013 (\pm)-7-[(1-(3,4-Dimethoxybenzyl)piperidin-3-yl)methoxy]-3,4-di-
1014 methyl-2H-chromen-2-one (**5i**). 3,4-Dimethyl-7-(piperidin-3-ylme-
1015 thoxy)-2H-chromen-2-one (0.12 g, 0.40 mmol) was dissolved under
1016 magnetic stirring with 1.3 mL of 1,2-dichloroethane in a flame-dried
1017 round-bottomed flask. 3,4-Dimethoxybenzaldehyde (0.66 g, 0.40
1018 mmol) and sodium triacetoxyborohydride (0.12 g, 0.56 mmol) were
1019 added, and the reaction mixture was left under magnetic stirring at
1020 room temperature and under nitrogen atmosphere overnight. After the
1021 removal of the solvent, the solid crude was purified through flash
1022 chromatography (gradient eluent: methanol in CH_2Cl_2 , 0% \rightarrow 10%).
1023 Yield: 45%; mp 62–64 °C (dec). ^1H NMR (300 MHz, DMSO- d_6) δ :
1024 1.16–1.18 (m, 1H), 1.42–1.51 (m, 1H), 1.59–1.64 (m, 1H), 1.69–
1025 1.77 (m, 1H), 1.83–1.99 (m, 3H), 2.05 (s, 3H), 2.34 (s, 3H), 2.60–
1026 2.67 (m, 1H), 2.77–2.83 (m, 1H), 3.31 (d, J = 13.5 Hz, 1H), 3.40 (d, J
1027 = 13.5 Hz, 1H), 3.67 (s, 3H), 3.70 (s, 3H), 3.92–3.94 (m, 2H), 6.74–
1028 6.77 (m, 1H), 6.82–6.84 (m, 2H), 6.86–6.90 (m, 2H), 7.65 (d, J = 8.5
1029 Hz, 1H). Anal. ($\text{C}_{26}\text{H}_{31}\text{NO}_5$) Calcd %: C, 71.37; H, 7.14; N, 3.20.
1030 Found %: C, 71.56; H, 7.10; N, 3.09.

1031 **General Procedure for the Synthesis of 7-(4- and 3-Bromoalky- 1032**
1033 **loxy)-3,4-dimethyl-2H-chromen-2-one 6a,b.** A Pyrex vessel was
1034 charged with a magnetic stirring and Weflon bar and then 7-
1035 hydroxy-3,4-dimethyl-2H-chromen-2-one (0.57 g, 3.0 mmol) and
1036 anhydrous potassium carbonate (0.83 g, 6.0 mmol) were suspended in
1037 acetone (10 mL). The suitable commercially available dibromoalkyl
1038 derivative (15 mmol) was added. The reactor was placed in a
1039 microwave apparatus and irradiated at 130 °C for 30 min. After
1040 cooling to room temperature, the solid residue was filtered and washed
1041 with CH_2Cl_2 . The solution was concentrated to dryness, and the
1042 resulting crude was purified through flash chromatography (gradient
1043 eluent as indicated below).

1044 7-(3-Bromopropoxy)-3,4-dimethyl-2H-chromen-2-one (**6a**). Puri-
1045 fied by flash chromatography (gradient eluent: ethyl acetate in n -
1046 hexane 0% \rightarrow 60%). Yield: 79%. ^1H NMR (500 MHz, DMSO- d_6) δ :
1047 2.07 (s, 3H), 2.27 (q, J = 6.4 Hz, 2H), 2.36 (s, 3H), 3.67 (t, J = 6.4 Hz,
1048 2H), 4.18 (t, J = 6.4 Hz, 2H), 6.95–6.98 (m, 2H), 7.70 (d, J = 8.8 Hz,
1049 1H).

1050 7-(4-Bromobutoxy)-3,4-dimethyl-2H-chromen-2-one (**6b**). Puri-
1051 fied by flash chromatography (gradient eluent: ethyl acetate in n -
1052 hexane 0% \rightarrow 50%). Yield: 88%. ^1H NMR (500 MHz, DMSO- d_6) δ :
1053 1.85 (qn, J = 6.4 Hz, 2H), 1.97 (qn, J = 6.4 Hz, 2H), 2.07 (s, 3H), 2.36
1054 (s, 3H), 3.61 (t, J = 6.4 Hz, 2H), 4.10 (t, J = 6.4 Hz, 2H), 6.92–6.95
1055 (m, 2H), 7.68 (d, J = 8.8 Hz, 1H).

1056 **General Procedure for the Synthesis of Final Compounds 7a,b.**
1057 Appropriate bromide derivative **6a,b** (0.50 mmol) was suspended
1058 under magnetic stirring in acetone (4 mL) in a Pyrex microwave
1059 reactor in the presence of anhydrous potassium carbonate (0.21 g, 1.5
1060 mmol) and catalytic amount of potassium iodide. 1,2,3,4-Tetrahy-
1061 droisoquinoline (0.080 g, 0.60 mmol) was added, and the vessel was
1062 placed in a microwave apparatus and heated at 130 °C for 45 min.
1063 After cooling to room temperature, the solid residue was filtered off
1064 after washing with CH_2Cl_2 . The solution was concentrated to dryness,
1065 and the resulting crude was purified through flash chromatography
1066 (gradient eluent: ethyl acetate in n -hexane 20% \rightarrow 80%). The resulting
1067 solids were transformed into the corresponding hydrochlorides by
1068 dissolving the base in the minimum amount of 1,4-dioxane followed by
1069 the addition of HCl 4.0 N in 1,4-dioxane. The precipitate was collected
1070 after filtration and washed with dry 1,4-dioxane under an Ar
1071 atmosphere.

1072 7-[3-(3,4-Dihydroisoquinolin-2(1H)-yl)propoxy]-3,4-dimethyl-2H-
1073 chromen-2-one Hydrochloride (**7a**). Yield: 74%; mp > 250 °C. ^1H
1074 NMR (free base, 300 MHz, DMSO- d_6) δ : 1.98 (qn, J = 6.4 Hz, 2H),
1075 2.05 (s, 3H), 2.34 (s, 3H), 2.59 (t, J = 6.4 Hz, 2H), 2.65 (t, J = 5.8 Hz,
1076 2H), 2.79 (t, J = 5.8 Hz, 2H), 3.55 (s, 2H), 4.13 (t, J = 6.4 Hz, 2H),
1077 6.91–6.94 (m, 2H), 7.01–7.09 (m, 4H), 7.66 (d, J = 9.9 Hz, 1H).
1078 Anal. ($\text{C}_{23}\text{H}_{25}\text{NO}_3\cdot\text{HCl}$) Calcd %: C, 69.08; H, 6.55; N, 3.50. Found
1079 %: C, 69.45; H, 6.58; N, 3.75.

1080 7-[4-(3,4-Dihydroisoquinolin-2(1H)-yl)butoxy]-3,4-dimethyl-2H-
1081 chromen-2-one hydrochloride (**7b**). Yield: 72%; mp 206–208 °C. ^1H

1082 NMR (free base, 500 MHz, DMSO- d_6) δ : 1.67 (qn, $J = 6.9$ Hz, 2H),
1083 1.79 (qn, $J = 6.9$ Hz, 2H), 2.07 (s, 3H), 2.36 (s, 3H), 2.46–2.48 (m,
1084 2H), 2.64 (t, $J = 5.4$ Hz, 2H), 2.79 (t, $J = 5.4$ Hz, 2H), 3.53 (s, 2H),
1085 4.10 (t, $J = 6.9$ Hz, 2H), 6.92–6.96 (m, 2H), 7.01–7.08 (m, 4H), 7.67
1086 (d, $J = 9.8$ Hz, 1H). Anal. ($C_{24}H_{27}NO_3 \cdot HCl$) Calcd %: C, 69.64; H,
1087 6.82; N, 3.38. Found %: C, 69.62; H, 6.79; N, 3.63.

1088 **HPLC Chiral Resolution.** HPLC chiral resolution of racemic **5b**
1089 and **5d** were performed on a Analytic Agilent 1260 Infinity
1090 multidetector system equipped with 1200 series UV-diode array
1091 detector using one of the following methods in a semipreparative polar
1092 mode at room temperature. UV spectra were recorded at 230, 254,
1093 280, and 320 nm. Twenty aliquots (100 μ L each) of the appropriate
1094 stock solutions (5 mg/mL in methanol for **5b** and 5 mg/mL in
1095 acetonitrile for **5d**) were injected. After collection and evaporation of
1096 the solvent, enantiomeric excess was measured with the same
1097 conditions as the separation. Method A (for **5b**): Chiralpak IA
1098 (Chiral Technologies Europe, 25 cm \times 0.46 cm I.D.); mobile phase, A
1099 = methanol, B = acetonitrile; isocratic solvent, 20% B; flow rate = 1
1100 mL/min; $\lambda = 320$ nm; 100 μ L injection. Method B (for **5d**): Chiralpak
1101 IA (Chiral Technologies Europe, 25 cm \times 0.46 cm I. D.); mobile
1102 phase, A = methanol, B = acetonitrile; isocratic solvent, 30% B; flow
1103 rate = 1 mL/min; $\lambda = 320$ nm; 100 μ L injection. Data were integrated
1104 and reported using OpenLAB software (Agilent Technologies). All
1105 compounds display enantiomeric excess >99% as determined by this
1106 method. Chromatographic analyses are reported in the [Supporting](#)
1107 [Information](#).

1108 **Volsurf+ Calculations.** Volsurf+ (Molecular Discovery, Perugia,
1109 Italy) was employed to compute different MIF-based⁵⁴ Log BB, a
1110 distribution parameter used to roughly assess the drug capability to
1111 cross the blood–brain barrier (BBB).^{46,76}

1112 **Aqueous Solubility Measurement: Turbidimetric Method.**
1113 The compound under study was dissolved in DMSO (at concentration
1114 of 2.5 and 30 mg/mL for **5b** as free base, 2 and 25 mg/mL for **1**,³⁴ **4j**,
1115 and **5a**) and added in portions to 50 mM Tris-HCl, pH 7.4, at room
1116 temperature. An Agilent 8453E UV–visible spectrophotometer
1117 equipped with a cell changer was used to detect light scattering
1118 produced by the addition of stock solutions to Tris-HCl buffer, and
1119 solubility calculations were performed as previously reported⁴⁶ from a
1120 bilinear curve fit in a plot of the absorbance (y axis) versus μ L of
1121 DMSO (x axis). Increased UV absorbance was measured in the 580–
1122 780 nm range. The solubility at pH 7.4 was the mean \pm SEM of three
1123 independent assays and was expressed as log S (mol/L).

1124 **RP-HPLC Determination of Lipophilicity Index (log k').** log k'
1125 determinations were carried out using a Zorbax Eclipse-C18 4.6 mm
1126 \times 250 mm, with 5 μ m size particles, built on a Waters double pump
1127 HPLC system in isocratic conditions. Injection volumes were 10 μ L,
1128 flow rate was 1 mL/min, and detection was performed with UV ($\lambda =$
1129 230 and 280 nm). Samples of compounds **1**, **4j**, **5a**, and **5b** were
1130 prepared in methanol at concentration 1 mM. The mobile phase was
1131 filtered through a Nylon-66 membrane 0.45 μ m (Supelco, USA)
1132 before use. log k' values were calculated using the following equation:

$$\log k' = \log[(t_r - t_0)/t_0]$$

1133 where retention times (t_r) were measured at least from three separate
1134 injections, and dead time (t_0) was the retention time of KI (1 mg/mL
1135 in methanol). The mobile phase consisted of different mixtures of
1136 methanol and ammonium acetate buffer (20 mM, pH 5.0): methanol/
1137 buffer 70% (v/v), methanol/buffer 65% (v/v), methanol/buffer 60%
1138 (v/v), methanol/buffer 55% (v/v), methanol/buffer 50% (v/v),
1139 methanol/buffer 45% (v/v).

1140 **Human Monoamine Oxidases Inhibition Assays.** Human
1141 monoamine oxidase inhibition assays were carried out with a
1142 fluorescence based method,^{34,56} using kynuramine as nonselective
1143 MAO A and MAO B substrate. Human recombinant MAO A and
1144 MAO B (microsomes from baculovirus infected insect cells; Sigma-
1145 Aldrich) were used. IC_{50} s for most active compounds were determined
1146 from seven concentrations ranging from 10^{-4} to 10^{-11} M. Reactions
1147 were performed in triplicates in black, round-bottomed polystyrene
1148 96-well microtiter plates (Greiner). Samples were preincubated 20 min
1149 at 37 $^{\circ}$ C before adding MAO solutions, then incubated for additional

30 min. Fluorescence was recorded at excitation/emission wavelengths
1150 of 320/400 nm (20 nm slit width for excitation, 30 nm slit width for
1151 emission) in a 96-well microplate fluorescence reader (Tecan Infinite
1152 M100 Pro). Inhibitory activities were determined by means of
1153 nonlinear regressions performed with GraphPad Prism 5.0 software
1154 and are expressed as IC_{50} (μ M) or as percentage of inhibition at 10
1155 μ M. Results are the mean of three independent experiments.

1156 **Electric Eel and Equine Serum Cholinesterases Inhibition**
1157 **Assays.** In vitro ChEs inhibition assays were performed on AChE
1158 from electric eel (463 U/mg; Sigma) and BChE from equine serum
1159 (13 U/mg; Sigma), according to the well-known spectrophotometric
1160 Ellman's method.⁵⁷ The experimental protocol for inhibition
1161 determination and kinetic studies has been adapted to a 96-well
1162 plate procedure from a previously reported method.⁷⁷ Inhibitory
1163 activities were determined by means of nonlinear regressions of the
1164 response/log(concentration) curve performed with GraphPad Prism
1165 5.0 and are reported as IC_{50} (μ M) or as percentage of inhibition at 10
1166 μ M for less active compounds. Experiments were performed in
1167 triplicates in transparent, flat-bottomed polystyrene 96-well microtiter
1168 plates. Seven concentrations of inhibitor, ranging from 10^{-4} to 10^{-10}
1169 M, were used; results are the mean of three independent experiments.
1170 Kinetic studies were performed with the same test conditions, using six
1171 concentrations of substrate (from 0.033 to 0.2 mM) and four
1172 concentrations of inhibitor (0 to 8 μ M). Apparent inhibition constants
1173 and kinetic parameters were calculated within the "Enzyme Kinetics"
1174 module of Prism.

1175 **Cytotoxicity Assays and Neuroprotection against Oxidative**
1176 **Stress Insults.** The cytotoxic damage produced by selected
1177 compounds and the ability to rescue cells from oxidative insults was
1178 investigated by following a protocol already described.³⁴ The viability
1179 of human neuroblastoma cells SH-SY5Y was determined through the
1180 MTT assay⁵⁸ in 96-well microtiter plates after 24 h incubation at 37
1181 $^{\circ}$ C with studied compounds at concentrations 0.1, 1, 5, 10, and 50 μ M
1182 and expressed as concentration responsible for 50% inhibition of cell
1183 growth (IC_{50}) or percentage of viable cells vs untreated cells (control).
1184 The absorbance at 570 nm was determined using a PerkinElmer 2030
1185 multilabel reader Victor TM X3. In the same cell lines, the protective
1186 effect of selected compounds and donepezil incubated for 24 h at two
1187 different concentrations (1 and 10 μ M) against three cytotoxic insults
1188 (H_2O_2 300 μ M, oligomycin-A 10 μ M, rotenone 20 μ M) was
1189 studied.^{34,78} Each compound was tested in triplicate, and the
1190 experiments were repeated three times. Cells incubated without
1191 insults and compounds were used as control. Data are determined
1192 through MTT assay and are expressed as percentage of viable cells vs
1193 untreated cells (control). Standard error of the mean (SD) is given.
1194 Statistical significance was determined using a two-way analysis of
1195 variance (ANOVA) followed by the Bonferroni post hoc tests
1196 (GraphPad Prism version 5) and was assigned to $p < 0.05$ (*) and
1197 $p < 0.01$ (**).

1198 **Bidirectional Transport Studies on MDCKII-MDR1 Mono-**
1199 **layers.** As previously reported,^{34,78} Madin–Darby canine kidney
1200 (MDCK) cells were retrovirally transfected with the human MDR1
1201 cDNA (MDCKII-MDR1).^{79,80} MDCKII-MDR1 cells were cultured in
1202 DMEM medium and seeded at a density of 100000 cell/cm² onto
1203 polyester 12-well Transwell inserts (pore size 0.4 μ m, 12 mm
1204 diameter, apical volume 0.5 mL, basolateral volume 1.5 mL).
1205 MDCKII-MDR1 cell barrier function was verified prior to the
1206 described transport experiments by measuring trans-epithelial electrical
1207 resistance (TEER) using an EVOM apparatus and the flux of
1208 fluorescein isothiocyanate-dextran (FD4, Sigma-Aldrich, Italy) (200
1209 μ g/mL) and diazepam (75 μ M). The analysis of compounds (\pm)-**5a**,**b**
1210 and (\pm)-**5e** were performed through UV–visible (Vis) spectroscopy
1211 using a PerkinElmer double-beam UV–visible spectrophotometer
1212 Lambda Bio 20 (Milan, Italy), equipped with 10 mm path-length-
1213 matched quartz cells. Standard calibration curves were prepared at
1214 maximum absorption wavelength of each compound using PBS as
1215 solvent and were linear ($r^2 = 0.999$) over the range of tested
1216 concentration (from 5 to 75 μ M). The FD4 samples were analyzed
1217 with a Victor3 fluorimeter (Wallac Victor3, 1420 Multilabel Counter,
1218 PerkinElmer) at excitation and emission wavelengths of 485 and 535
1219

1220 nm, respectively. Each compound was tested in triplicate, and the
1221 experiments were repeated three times. Data are reported as the
1222 apparent permeability (P_{app}), in units of cm/s, determined as indicated
1223 in the following equation:

$$P_{app} = \left(\frac{V_A}{\text{area} \times \text{time}} \right) \times \left(\frac{[\text{drug}]_{\text{acceptor}}}{[\text{drug}]_{\text{initial}}} \right)$$

1224 where " V_A " is the volume in the acceptor well, "area" is the surface area
1225 of the membrane, "time" is the total transport time, " $[\text{drug}]_{\text{acceptor}}$ " is
1226 the concentration of the drug measured by UV-spectroscopy, and
1227 " $[\text{drug}]_{\text{initial}}$ " is the initial drug concentration in the AP or BL chamber.
1228 Efflux ratio (ER) was calculated using the following equation: ER =
1229 $P_{app, \text{BL-AP}}/P_{app, \text{AP-BL}}$, where $P_{app, \text{BL-AP}}$ is the apparent
1230 permeability of basal-to-apical transport, and $P_{app, \text{AP-BL}}$ is the
1231 apparent permeability of apical-to-basal transport. An efflux ratio
1232 greater than 2 indicates that a test compound is likely to be a substrate
1233 for P-gp transport.

1234 ■ ASSOCIATED CONTENT

1235 ● Supporting Information

1236 The Supporting Information is available free of charge on the
1237 ACS Publications website at DOI: [10.1021/acs.jmed-](https://doi.org/10.1021/acs.jmedchem.6b00562)
1238 [chem.6b00562](https://doi.org/10.1021/acs.jmedchem.6b00562).

1239 Applicability domain for Volsurf+ predictions; chiral-
1240 HPLC analysis on enantiomeric excess for (+)-**5b**,
1241 (–)-**5b**, (+)-**5d**, and (–)-**5d**; protocols of MAOs and
1242 ChEs inhibition assays (PDF)

1243 ■ AUTHOR INFORMATION

1244 Corresponding Author

1245 *Phone: +39-0805442780. Fax: +39-080-5442230. E-mail:
1246 marco.catto@uniba.it.

1247 Notes

1248 The authors declare no competing financial interest.

1249 ■ ACKNOWLEDGMENTS

1250 The financial support from MIUR, Italy (Grant Futuro in
1251 Ricerca 2012, RBFRI2SJA8_003) is kindly acknowledged.

1252 ■ ABBREVIATIONS USED

1253 BBB, blood–brain barrier; CAS, catalytic anionic; FAD, flavin
1254 adenine dinucleotide; FD4, fluorescein isothiocyanate-dextran;
1255 MDCKII-MDR1, Madin–Darby canine kidney cells retrovirally
1256 transfected with the human MDR1 cDNA; MIF, molecular
1257 interaction field; MTDL, multitarget directed ligand; MTT, 3-
1258 (4,5-dimethylthiazol-2-yl)-2,5-diphenyltetrazolium bromide;
1259 P_{app} , apparent permeability; $P_{app, \text{AP-BL}}$, apparent permeability
1260 apical-to-basal; $P_{app, \text{BL-AP}}$, apparent permeability basal-to-
1261 apical; PAS, peripheral anionic binding site; P-gp, P-
1262 glycoprotein; ROS, reactive oxygen species; SAR, structure–
1263 activity relationships; TEER, trans-epithelial electrical resistance

1264 ■ REFERENCES

1265 (1) Wimo, A.; Jonsson, L.; Bond, J.; Prince, M.; Winblad, B. The
1266 Worldwide Economic Impact of Dementia 2010. *Alzheimer's Dementia*
1267 **2013**, *9*, 1–11.
1268 (2) Querfurth, H. W.; LaFerla, F. M. Alzheimer's Disease. *N. Engl. J.*
1269 *Med.* **2010**, *362*, 329–344.
1270 (3) Cummings, J. L.; Morstorf, T.; Zhong, K. Alzheimer's Disease
1271 Drug-development Pipeline: Few Candidates, Frequent Failures.
1272 *Alzheimer's Res. Ther.* **2014**, *6*, 37.

(4) Berk, C.; Sabbagh, M. N. Successes and Failures for Drugs in
1273 Late-stage Development for Alzheimer's Disease. *Drugs Aging* **2013**,
1274 *30*, 783–792.

(5) Narayan, P.; Ehsani, S.; Lindquist, S. Combating Neuro-
1275 degenerative Disease with Chemical Probes and Model Systems.
1276 *Nat. Chem. Biol.* **2014**, *10*, 911–920.
1278

(6) Bush, A. I. The Metal Theory of Alzheimer's Disease. *J.*
1279 *Alzheimer's Dis.* **2013**, *33*, S277–S281.
1280

(7) Zhao, Y.; Zhao, B. Oxidative Stress and the Pathogenesis of
1281 Alzheimer's Disease. *Oxid. Med. Cell. Longevity* **2013**, *2013*, 316523.
1282

(8) Terry, A. V., Jr.; Buccafusco, J. J. The Cholinergic Hypothesis of
1283 Age and Alzheimer's Disease-related Cognitive Deficits: Recent
1284 Challenges and Their Implications for Novel Drug Development. *J.*
1285 *Pharmacol. Exp. Ther.* **2003**, *306*, 821–827.
1286

(9) Johnson, J. W.; Kotermanski, S. E. Mechanism of Action of
1287 Memantine. *Curr. Opin. Pharmacol.* **2006**, *6*, 61–67.
1288

(10) Muñoz-Torrero, D. Acetylcholinesterase Inhibitors as Disease
1289 Modifying Therapies for Alzheimer's Disease. *Curr. Med. Chem.* **2008**,
1290 *15*, 2433–2455.
1291

(11) Zimmermann, G. R.; Lehár, J.; Keith, C. T. Multi-target
1292 Therapeutics: When the Whole is Greater than the Sum of the Parts.
1293 *Drug Discovery Today* **2007**, *12*, 34–42.
1294

(12) Leon, R.; Garcia, A. G.; Marco-Contelles, J. Recent Advances in
1295 the Multitarget-Directed Ligands Approach for the Treatment of
1296 Alzheimer's Disease. *Med. Res. Rev.* **2013**, *33*, 139–189.
1297

(13) Lee, S.; Zheng, X.; Krishnamoorthy, J.; Savelieff, M. G.; Park, H.
1298 M.; Brender, J. R.; Kim, J. H.; Derrick, J. S.; Kochi, A.; Lee, H. J.; Kim,
1299 C.; Ramamoorthy, A.; Bowers, M. T.; Lim, M. H. Rational Design of a
1300 Structural Framework with Potential Use to Develop Chemical
1301 Reagents that Target and Modulate Multiple Facets of Alzheimer's
1302 Disease. *J. Am. Chem. Soc.* **2014**, *136*, 299–310.
1303

(14) Prati, F.; De Simone, A.; Bisignano, P.; Armirotti, A.; Summa,
1304 M.; Pizzirani, D.; Scarpelli, R.; Perez, D. I.; Andrisano, V.; Perez-
1305 Castillo, A.; Monti, B.; Massenzio, F.; Polito, L.; Racchi, M.; Favia, A.
1306 D.; Bottegoni, G.; Martinez, A.; Bolognesi, M. L.; Cavalli, A.
1307 Multitarget Drug Discovery for Alzheimer's Disease: Triazinones as
1308 BACE-1 and GSK-3 β Inhibitors. *Angew. Chem., Int. Ed.* **2015**, *54*,
1309 1578–1582.
1310

(15) Zheng, H.; Youdim, M. B. H.; Fridkin, M. Site-activated
1311 Chelators Targeting Acetylcholinesterase and Monoamine Oxidase for
1312 Alzheimer's Therapy. *ACS Chem. Biol.* **2010**, *5*, 603–610.
1313

(16) Rochais, C.; Lecoutey, C.; Gaven, F.; Giannoni, P.;
1314 Hamidouche, K.; Hedou, D.; Dubost, E.; Genest, D.; Yahiaoui, S.;
1315 Freret, T.; Bouet, V.; Dauphin, F.; Sopkova de Oliveira Santos, J.;
1316 Ballandonne, C.; Corvaisier, S.; Malzert-Fréon, A.; Legay, R.;
1317 Boulouard, M.; Claeysen, S.; Dallemagne, P. Novel Multitarget-
1318 directed Ligands (MTDLs) with Acetylcholinesterase (AChE)
1319 Inhibitory and Serotonergic Subtype 4 Receptor (5-HT4R) Agonist
1320 Activities as Potential Agents against Alzheimer's Disease: the Design
1321 of Donecopride. *J. Med. Chem.* **2015**, *58*, 3172–3187.
1322

(17) Pau, A.; Catto, M.; Pinna, G.; Frau, S.; Murineddu, G.; Asproni,
1323 B.; Curzu, M. M.; Pisani, L.; Leonetti, F.; Loza, M. I.; Brea, J.; Pinna,
1324 G. A.; Carotti, A. Multitarget-directed Tricyclic Pyridazinones as
1325 Ligands of Selected G-protein Coupled Receptors and Inhibitors of
1326 Cholinesterases. *ChemMedChem* **2015**, *10*, 1054–1070.
1327

(18) Fernández-Bachiller, M. I.; Pérez, C.; Monjas, L.; Rademann, J.;
1328 Rodríguez-Franco, M. I. New Tacrine–4-Oxo-4H-chromene Hybrids
1329 as Multifunctional Agents for the Treatment of Alzheimer's Disease,
1330 with Cholinergic, Antioxidant, and β -Amyloid-Reducing Properties. *J.*
1331 *Med. Chem.* **2012**, *55*, 1303–1317.
1332

(19) Chen, Y.; Sun, J.; Fang, L.; Liu, M.; Peng, S.; Liao, H.; Lehmann,
1333 J.; Zhang, Y. Tacrine–Ferulic Acid–Nitric Oxide (NO) Donor
1334 Trihybrids as Potent, Multifunctional Acetyl- and Butyrylcholinester-
1335 ase Inhibitors. *J. Med. Chem.* **2012**, *55*, 4309–4321.
1336

(20) Fang, L.; Appenroth, D.; Decker, M.; Kiehnopf, M.; Lupp, A.;
1337 Peng, S.; Fleck, C.; Zhang, Y.; Lehmann, J. NO-Donating Tacrine
1338 Hybrid Compounds Improve Scopolamine-Induced Cognition Impair-
1339 ment and Show Less Hepatotoxicity. *J. Med. Chem.* **2008**, *51*, 7666–
1340 7669.
1341

- 1342 (21) Dvir, H.; Silman, I.; Harel, M.; Rosenberry, T. L.; Sussman, J. L.
1343 Acetylcholinesterase: From 3D Structure to Function. *Chem.-Biol.*
1344 *Interact.* **2010**, *187*, 10–22.
- 1345 (22) Harel, M.; Schalk, L.; Ehret-Sabatier, L.; Bouet, F.; Goeldner, M.;
1346 Hirth, C.; Axelsen, P. H.; Silman, I.; Sussman, J. L. Quaternary Ligand
1347 Binding to Aromatic Residues in the Active-site Gorge of
1348 Acetylcholinesterase. *Proc. Natl. Acad. Sci. U. S. A.* **1993**, *90*, 9031–
1349 9035.
- 1350 (23) Inestrosa, N. C.; Alvarez, A.; Pérez, C. A.; Moreno, R. D.;
1351 Vicente, M.; Linker, C.; Casanueva, O. I.; Soto, C.; Garrido, J.
1352 Acetylcholinesterase Accelerates Assembly of Amyloid- β -peptides into
1353 Alzheimer's Fibrils: Possible Role of the Peripheral Site of the Enzyme.
1354 *Neuron* **1996**, *16*, 881–891.
- 1355 (24) Lockridge, O. Review of Human Butyrylcholinesterase
1356 Structure, Function, Genetic Variants, History of Use in the Clinic,
1357 and Potential Therapeutic Uses. *Pharmacol. Ther.* **2015**, *148*, 34–46.
- 1358 (25) Lane, R. M.; Potkin, S. G.; Enz, A. Targeting Acetylcholinesterase
1359 and Butyrylcholinesterase in Dementia. *Int. J. Neuropsychopharma-*
1360 *col.* **2006**, *9*, 101–124.
- 1361 (26) Giacobini, E. Selective Inhibitors of Butyrylcholinesterase: a
1362 Valid Alternative for Therapy of Alzheimer's Disease? *Drugs Aging*
1363 **2001**, *18*, 891–898.
- 1364 (27) Riederer, P.; Danielczyk, W.; Gruenblatt, E. Monoamine
1365 Oxidase-B Inhibition in Alzheimer's Disease. *NeuroToxicology* **2004**,
1366 *25*, 271–277.
- 1367 (28) De Colibus, L.; Li, M.; Binda, C.; Lustig, A.; Edmondson, D. E.;
1368 Mattevi, A. Three-Dimensional Structure of Human Monoamine
1369 Oxidase A (MAO A): Relation to the Structures of Rat MAO A and
1370 Human MAO B. *Proc. Natl. Acad. Sci. U. S. A.* **2005**, *102*, 12684–
1371 12689.
- 1372 (29) Binda, C.; Newton-Vinson, P.; Hubalek, F.; Edmondson, D. E.;
1373 Mattevi, A. Structure of Human Monoamine Oxidase B, a Drug Target
1374 for the Treatment of Neurological Disorders. *Nat. Struct. Biol.* **2002**, *9*,
1375 22–26.
- 1376 (30) Rapaport, M. H. Dietary Restrictions and Drug Interactions
1377 with Monoamine Oxidase Inhibitors: the State of the Art. *J. Clin.*
1378 *Psychiatry* **2007**, *68*, 42–46.
- 1379 (31) Wimbiscus, M.; Kostenko, O.; Malone, D. MAO Inhibitors:
1380 Risks, Benefits, and Lore. *Cleve. Clin. J. Med.* **2010**, *77*, 859–882.
- 1381 (32) Barnham, K. J.; Masters, C. L.; Bush, A. I. Neurodegenerative
1382 Diseases and Oxidative Stress. *Nat. Rev. Drug Discovery* **2004**, *3*, 205–
1383 214.
- 1384 (33) Tonelli, M.; Catto, M.; Tasso, B.; Novelli, F.; Canu, C.; Iusco,
1385 G.; Pisani, L.; De Stradis, A.; Denora, N.; Sparatore, A.; Boido, V.;
1386 Carotti, A.; Sparatore, F. Multitarget Therapeutic Leads for
1387 Alzheimer's disease. Quinolizidinyl Derivatives of Bi- and Tri-cyclic
1388 Systems as Dual Inhibitors of Cholinesterases and A β Aggregation.
1389 *ChemMedChem* **2015**, *10*, 1040–1053.
- 1390 (34) Farina, R.; Pisani, L.; Catto, M.; Nicolotti, O.; Gadaleta, D.;
1391 Denora, N.; Soto-Otero, R.; Mendez-Alvarez, E.; Passos, C. S.;
1392 Muncipinto, G.; Altomare, C. D.; Nurisso, A.; Carrupt, P. A.; Carotti,
1393 A. Structure-Based Design and Optimization of Multitarget-Directed
1394 2H-Chromen-2-one Derivatives as Potent Inhibitors of Monoamine
1395 Oxidase B and Cholinesterases. *J. Med. Chem.* **2015**, *58*, 5561–5578.
- 1396 (35) Matos, M. J.; Terán, C.; Pérez-Castillo, Y.; Uriarte, E.; Santana,
1397 L.; Viña, D. Synthesis and Study of a Series of 3-Arylcoumarins as
1398 Potent and Selective Monoamine Oxidase B Inhibitors. *J. Med. Chem.*
1399 **2011**, *54*, 7127–7137.
- 1400 (36) Mertens, M. D.; Hinz, S.; Müller, C. E.; Gütschow, M. Alkynyl-
1401 coumarinyl Ethers as MAO-B Inhibitors. *Bioorg. Med. Chem.* **2014**, *22*,
1402 1916–1928.
- 1403 (37) Secci, D.; Carradori, S.; Bolasco, A.; Chimenti, P.; Yáñez, M.;
1404 Ortuso, F.; Alcaro, S. Synthesis and Selective Human Monoamine
1405 Oxidase Inhibition of 3-Carbonyl, 3-Acyl, and 3-Carboxyhydrazido
1406 Coumarin Derivatives. *Eur. J. Med. Chem.* **2011**, *46*, 4846–4852.
- 1407 (38) Patil, P. O.; Bari, S. B.; Firke, S. D.; Deshmukh, P. K.; Donda, S.
1408 T.; Patil, D. A. A Comprehensive Review on Synthesis and Designing
1409 Aspects of Coumarin Derivatives as Monoamine Oxidase Inhibitors for
Depression and Alzheimer's Disease. *Bioorg. Med. Chem.* **2013**, *21*, 1410
2434–2450. 1411
- (39) Delogu, G.; Picciau, C.; Ferino, G.; Quezada, E.; Podda, G.;
1412 Uriarte, E.; Viña, D. Synthesis, Human Monoamine Oxidase Inhibitory
1413 Activity and Molecular Docking Studies of 3-Heteroaryl Coumarin
1414 Derivatives. *Eur. J. Med. Chem.* **2011**, *46*, 1147–1152. 1415
- (40) Catto, M.; Pisani, L.; Leonetti, F.; Nicolotti, O.; Pesce, P.;
1416 Stefanachi, A.; Cellamare, S.; Carotti, A. Design, Synthesis and
1417 Biological Evaluation of Coumarin Alkylamines as Potent and Selective
1418 Dual Binding Site Inhibitors of Acetylcholinesterase. *Bioorg. Med.*
1419 *Chem.* **2013**, *21*, 146–152. 1420
- (41) Alipour, M.; Khoobi, M.; Moradi, A.; Nadri, H.; Moghadam, F.
1421 H.; Emami, S.; Hasanpour, Z.; Foroumadi, A.; Shafiee, A. Synthesis
1422 and Anti-cholinesterase Activity of New 7-Hydroxycoumarin Deriva-
1423 tives. *Eur. J. Med. Chem.* **2014**, *82*, 536–544. 1424
- (42) Pisani, L.; Catto, M.; Giangreco, I.; Leonetti, F.; Nicolotti, O.;
1425 Stefanachi, A.; Cellamare, S.; Carotti, A. Design, Synthesis and
1426 Biological Evaluation of Coumarin Derivatives Tethered to an
1427 Edrophonium-like Fragment as Highly Potent and Selective Dual
1428 Binding Site Acetylcholinesterase Inhibitors. *ChemMedChem* **2010**, *5*,
1429 1616–1630. 1430
- (43) Wang, Z.-M.; Li, X.-M.; Xue, G.-M.; Xu, W.; Wang, X.-B.; Kong,
1431 L.-Y. Synthesis and Evaluation of 6-Substituted 3-Arylcoumarin
1432 Derivatives as Multifunctional Acetylcholinesterase/monoamine Oxi-
1433 dase B Dual Inhibitors for the Treatment of Alzheimer's Disease. *RSC*
1434 *Adv.* **2015**, *5*, 104122–104137. 1435
- (44) Xie, S.-S.; Wang, X.; Jiang, N.; Yu, W.; Wang, K. D. G.; Lan, J.-
1436 S.; Li, Z.-R.; Kong, L.-Y. Multi-target Tacrine-coumarin Hybrids:
1437 Cholinesterase and Monoamine Oxidase B Inhibition Properties
1438 against Alzheimer's Disease. *Eur. J. Med. Chem.* **2015**, *95*, 153–165. 1439
- (45) Jameel, E.; Umar, T.; Kumar, J.; Hoda, N. Coumarin: A
1440 Privileged Scaffold for the Design and Development of Antineur-
1441 odegenerative Agents. *Chem. Biol. Drug Des.* **2016**, *87*, 21–38. 1442
- (46) Pisani, L.; Muncipinto, G.; Miscioscia, T. F.; Nicolotti, O.;
1443 Leonetti, F.; Catto, M.; Caccia, C.; Salvati, P.; Soto-Otero, R.; Mendez-
1444 Alvarez, E.; Passeleu, C.; Carotti, A. Discovery of a Novel Class of
1445 Potent Coumarin Monoamine Oxidase B Inhibitors: Development and
1446 Biopharmacological Profiling of 7-[(3-Chlorobenzyl)oxy]-4-
1447 [(methylamino)methyl]-2H-chromen-2-one Methanesulfonate (NW-
1448 1772) as a Highly Potent, Selective, Reversible, and Orally Active
1449 Monoamine Oxidase B Inhibitor. *J. Med. Chem.* **2009**, *52*, 6685–6706. 1450
- (47) Pisani, L.; Barletta, M.; Soto-Otero, R.; Nicolotti, O.; Mendez-
1451 Alvarez, E.; Catto, M.; Introcaso, A.; Stefanachi, A.; Cellamare, S.;
1452 Altomare, C.; Carotti, A. Discovery, Biological Evaluation, and
1453 Structure–Activity and – Selectivity Relationships of 6'-Substituted
1454 (E)-2-(Benzofuran-3(2H)-ylidene)-N-methylacetamides, a Novel
1455 Class of Potent and Selective Monoamine Oxidase Inhibitors. *J.*
1456 *Med. Chem.* **2013**, *56*, 2651–2664. 1457
- (48) Catto, M.; Nicolotti, O.; Leonetti, F.; Carotti, A.; Favia, A. D.;
1458 Soto-Otero, R.; Mendez-Alvarez, E.; Carotti, A. Structural Insights into
1459 Monoamine Oxidase Inhibitory Potency and Selectivity of 7-
1460 Substituted Coumarins from Ligand- and Target-Based Approaches.
1461 *J. Med. Chem.* **2006**, *49*, 4912–4925. 1462
- (49) Carotti, A.; Altomare, C.; Catto, M.; Gnerre, C.; Summo, L.; De
1463 Marco, A.; Rose, S.; Jenner, P.; Testa, B. Lipophilicity Plays a Major
1464 Role in Modulating Monoamine Oxidase B (MAO-B). Inhibition by 7-
1465 Substituted Coumarins. *Chem. Biodiversity* **2006**, *3*, 134–144. 1466
- (50) Pisani, L.; Catto, M.; Nicolotti, O.; Grossi, G.; Di Braccio, M.;
1467 Soto-Otero, R.; Mendez-Alvarez, E.; Stefanachi, A.; Gadaleta, D.;
1468 Carotti, A. Fine Molecular Tuning at Position 4 of 2H-Chromen-2-one
1469 Derivatives in the Search of Potent and Selective Monoamine Oxidase
1470 B Inhibitors. *Eur. J. Med. Chem.* **2013**, *70*, 723–739. 1471
- (51) Cheung, J.; Rudolph, M. J.; Burshteyn, F.; Cassidy, M. S.; Gary,
1472 E. N.; Love, J.; Franklin, M. C.; Height, J. J. Structures of Human
1473 Acetylcholinesterase in Complex with Pharmacologically Important
1474 Ligands. *J. Med. Chem.* **2012**, *55*, 10282–10286. 1475
- (52) Pisani, L.; Farina, R.; Nicolotti, O.; Gadaleta, D.; Soto-Otero, R.;
1476 Catto, M.; Di Braccio, M.; Mendez-Alvarez, E.; Carotti, A. In Silico
1477

- 1478 Design of Novel 2H-Chromen-2-one Derivatives as Potent and
1479 Selective MAO-B Inhibitors. *Eur. J. Med. Chem.* **2015**, *89*, 98–105.
- 1480 (53) Bruhlmann, C.; Ooms, F.; Carrupt, P. A.; Testa, B.; Catto, M.;
1481 Leonetti, F.; Altomare, C.; Carotti, A. Coumarins Derivatives as Dual
1482 Inhibitors of Acetylcholinesterase and Monoamine Oxidase. *J. Med.*
1483 *Chem.* **2001**, *44*, 3195–3198.
- 1484 (54) Cruciani, G.; Crivori, P.; Carrupt, P. A.; Testa, B. Molecular
1485 Fields in Quantitative Structure-Permeation Relationships: The
1486 VolSurf Approach. *J. Mol. Struct.: THEOCHEM* **2000**, *503*, 17–30.
- 1487 (55) Gnerre, C.; Catto, M.; Leonetti, F.; Weber, P.; Carrupt, P.-A.;
1488 Altomare, C.; Carotti, A.; Testa, B. Inhibition of Monoamine Oxidases
1489 by Functionalized Coumarin Derivatives: Biological Activities, QSARs,
1490 and 3D-QSARs. *J. Med. Chem.* **2000**, *43*, 4747–4758.
- 1491 (56) Novaroli, L.; Daina, A.; Favre, E.; Bravo, J.; Carotti, A.; Leonetti,
1492 F.; Catto, M.; Carrupt, P.-A.; Reist, M. Impact of Species-dependent
1493 Differences on Screening, Design, and Development of MAO-B
1494 Inhibitors. *J. Med. Chem.* **2006**, *49*, 6264–6272.
- 1495 (57) Ellman, G. L.; Courtney, K. D.; Andres, V., Jr.; Featherstone, R.
1496 M. A New and Rapid Colorimetric Determination of Acetylcholin-
1497 terase Activity. *Biochem. Pharmacol.* **1961**, *7*, 88–95.
- 1498 (58) Denizot, F.; Lang, R. Rapid Colorimetric Assay for Cell Growth
1499 and Survival. Modifications to the Tetrazolium Dye Procedure Giving
1500 Improved Sensitivity and Reliability. *J. Immunol. Methods* **1986**, *89*,
1501 271–277.
- 1502 (59) Denora, N.; Laquintana, V.; Lopalco, A.; Iacobazzi, R. M.;
1503 Lopodota, A.; Cutrignelli, A.; Iacobellis, G.; Annese, C.; Cascione, M.;
1504 Leporatti, S.; Franco, M. In vitro targeting and imaging of the
1505 translocator protein TSPO 18-kDa through G(4)-PAMAM-FITC
1506 labeled dendrimer. *J. Controlled Release* **2013**, *172*, 1111–1125.
- 1507 (60) Crivori, P.; Cruciani, G.; Carrupt, P. A.; Testa, B. Predicting
1508 Blood-Brain Barrier Permeation from Three-Dimensional Molecular
1509 Structure. *J. Med. Chem.* **2000**, *43*, 2204–2216.
- 1510 (61) (a) Tropsha, A.; Gramatica, P.; Gombar, V. The Importance of
1511 Being Earnest: Validation is the Absolute Essential for Successful
1512 Application and Interpretation of QSPR Models. *QSAR Comb. Sci.*
1513 **2003**, *22*, 69–77. (b) Eriksson, L.; Jaworska, J.; Worth, A.; Cronin, M.
1514 T. D.; McDowell, R. M.; Gramatica, P. Methods for Reliability and
1515 Uncertainty Assessment and for Applicability Evaluations of
1516 Classification- and Regression- Based QSARs. *Environ. Health Perspect.*
1517 **2003**, *111*, 1351–1375.
- 1518 (62) Li, N.; Ragheb, K.; Lawler, G.; Sturgis, J.; Rajwa, B.; Melendez,
1519 A. J.; Robinson, J. P. Mitochondrial Complex I Inhibitor Rotenone
1520 Induces Apoptosis through Enhancing Mitochondrial Reactive Oxygen
1521 Species Production. *J. Biol. Chem.* **2003**, *278*, 8516–8525.
- 1522 (63) Shchepina, L. A.; Pletjushkina, O. Y.; Avetisyan, A. V.; Bakeeva,
1523 L. E.; Fetisova, E. K.; Izyumov, D. S.; Saprunova, V. B.; Vyssokikh, M.
1524 Y.; Chernyak, B. V.; Skulachev, V. P. Oligomycin, Inhibitor of the F0
1525 Part of H⁺-ATP-synthase, Suppresses the TNF-induced Apoptosis.
1526 *Oncogene* **2002**, *21*, 8149–8157.
- 1527 (64) Rankovic, Z. CNS Drug Design: Balancing Physicochemical
1528 Properties for Optimal Brain Exposure. *J. Med. Chem.* **2015**, *58*, 2584–
1529 2608.
- 1530 (65) Pajouhesh, H.; Lenz, G. R. Medicinal Chemical Properties of
1531 Successful Central Nervous System Drugs. *NeuroRx* **2005**, *2*, 541–
1532 553.
- 1533 (66) Fernandez-Bachiller, M. I.; Perez, C.; Monjas, L.; Rademann, J.;
1534 Rodríguez-Franco, M. I. New Tacrine–4-Oxo-4H-chromene Hybrids
1535 as Multifunctional Agents for the Treatment of Alzheimer's Disease,
1536 with Cholinergic, Antioxidant, and β -Amyloid-Reducing Properties. *J.*
1537 *Med. Chem.* **2012**, *55*, 1303–1317.
- 1538 (67) Otto, R.; Penzis, R.; Gaube, F.; Adolph, O.; Fohr, K. J.;
1539 Warncke, P.; Robaa, D.; Appenroth, D.; Fleck, C.; Enzensperger, C.;
1540 Lehmann, J.; Winckler, T. Evaluation of Homobivalent Carbonylones as
1541 Designed Multiple Ligands for the Treatment of Neurodegenerative
1542 Disorders. *J. Med. Chem.* **2015**, *58*, 6710–6715.
- 1543 (68) Di Pietro, O.; Pérez-Areales, F. J.; Juárez-Jiménez, J.; Espargaró,
1544 A.; Clos, M. V.; Pérez, B.; Lavilla, R.; Sabaté, R.; Luque, F. J.; Muñoz-
1545 Torro, D. Tetrahydrobenzo[h][1,6]naphthyridine-6-chlorotacrine
1546 Hybrids as a New Family of Anti-Alzheimer Agents Targeting β -
Amyloid, Tau, and Cholinesterase Pathologies. *Eur. J. Med. Chem.* **2014**, *84*, 107–117.
- (69) Viayna, E.; Sola, I.; Bartolini, M.; De Simone, A.; Tapia-Rojas,
C.; Serrano, F. G.; Sabaté, R.; Juárez-Jiménez, J.; Perez, B.; Luque, F. J.;
Andrisano, V.; Clos, M. V.; Inestrosa, N. C.; Muñoz-Torero, D.
Synthesis and Multitarget Biological Profiling of a Novel Family of
Rhein Derivatives As Disease-Modifying Anti-Alzheimer Agents. *J.*
Med. Chem. **2014**, *57*, 2549–2567.
- (70) Wu, M.; Esteban, G.; Brogi, S.; Shionoya, M.; Wang, L.;
Campiani, G.; Unzeta, M.; Inokuchi, T.; Butini, S.; Marco-Contelles, J.
Donepezil-like Multifunctional Agents: Design, Synthesis, Molecular
Modeling and Biological Evaluation. *Eur. J. Med. Chem.* **2015**,
DOI:10.1016/j.ejmech.2015.10.001.
- (71) Wang, L.; Esteban, G.; Ojima, M.; Bautista-Aguilera, O. M.;
Inokuchi, T.; Moraleda, I.; Iriepa, I.; Samadi, A.; Youdim, M. B. H.;
Romero, A.; Soriano, E.; Herrero, R.; Fernández Fernández, A. P.;
Martínez-Murillo, R.; Marco-Contelles, J.; Unzeta, M. Donepezil +
Propargylamine + 8-Hydroxyquinoline Hybrids as New Multifunc-
tional Metal-chelators, ChE and MAO Inhibitors for the Potential
Treatment of Alzheimer's Disease. *Eur. J. Med. Chem.* **2014**, *80*, 543–
561.
- (72) Weinstock, M.; Bejar, C.; Wang, R. H.; Poltyrev, T.; Gross, A.;
Finberg, J. P.; Youdim, M. B. TV3326, a Novel Neuroprotective Drug
with Cholinesterase and Monoamine Oxidase Inhibitory Activities for
the Treatment of Alzheimer's Disease. *J. Neural Transm. Suppl.* **2000**,
60, 157–169.
- (73) Sterling, J.; Herzig, Y.; Goren, T.; Finkelstein, N.; Lerner, D.;
Goldenberg, W.; Miskolczi, I.; Molnar, S.; Rantal, F.; Tamas, T.; Toth,
G.; Zagya, A.; Zekany, A.; Lavian, G.; Gross, A.; Friedman, R.; Razin,
M.; Huang, W.; Kraiss, B.; Chovre, M.; Youdim, M. B. H.; Weinstock,
M. Novel Dual Inhibitors of AChE and MAO Derived from Hydroxy
Aminoindan and Phenethylamine as Potential Treatment for
Alzheimer's Disease. *J. Med. Chem.* **2002**, *45*, 5260–5279.
- (74) Avraham Pharmaceuticals Announces Successful Second
Interim Results in Phase 2b Study of Ladostigil for the Treatment
of Mild Cognitive Impairment, *Business Wire* July 28, 2015, [http://](http://www.businesswire.com/news/home/20150728005672/en/Avraham-Pharmaceuticals-Announces-Successful-Interim-Results-Phase)
[www.businesswire.com/news/home/20150728005672/en/Avraham-](http://www.businesswire.com/news/home/20150728005672/en/Avraham-Pharmaceuticals-Announces-Successful-Interim-Results-Phase)
[Pharmaceuticals-Announces-Successful-Interim-Results-Phase.](http://www.businesswire.com/news/home/20150728005672/en/Avraham-Pharmaceuticals-Announces-Successful-Interim-Results-Phase)
- (75) Anderson, M. C.; Hasan, F.; McCrodden, J. M.; Tipton, K. F.
Monoamine Oxidase Inhibitors and the Cheese Effect. *Neurochem. Res.*
1993, *18*, 1145–1149.
- (76) Lobell, M.; Molnár, L.; Keserü, G. M. Recent Advances in the
Prediction of Blood–brain Partitioning from Molecular Structure. *J.*
Pharm. Sci. **2003**, *92*, 360–370.
- (77) Conejo-García, A.; Pisani, L.; Núñez, M. C.; Catto, M.;
Nicolotti, O.; Leonetti, F.; Campos, J. M.; Gallo, M. A.; Espinosa, A.;
Carotti, A. Homodimeric bis-Quaternary Heterocyclic Ammonium
Salts as Potent Acetyl- and Butyryl-cholinesterase Inhibitors: A
Systematic Investigation of the Influence of Linker and Cationic
Heads Over Affinity and Selectivity. *J. Med. Chem.* **2011**, *54*, 2627–
2645.
- (78) Pisani, L.; Farina, R.; Soto-Otero, R.; Denora, N.; Mangiatordi,
G. F.; Nicolotti, O.; Mendez-Alvarez, E.; Altomare, C. D.; Catto, M.;
Carotti, A. Searching for Multi-Targeting Neurotherapeutics against
Alzheimer's: Discovery of Potent AChE-MAO B Inhibitors through
the Decoration of the 2H Chromen-2-one Structural Motif. *Molecules*
2016, *21*, 362.
- (79) Denora, N.; Laquintana, V.; Trapani, A.; Lopodota, A.; Latrofa,
A.; Gallo, J. M.; Trapani, G. Translocator Protein (TSPO) Ligand-Ara-
C (Cytarabine) Conjugates as a Strategy to Deliver Antineoplastic
Drugs and to Enhance Drug Clinical Potential. *Mol. Pharmaceutics*
2010, *7*, 2255–2269.
- (80) Denora, N.; Cassano, T.; Laquintana, V.; Lopalco, A.; Trapani,
A.; Cimmino, C. S.; Laconca, L.; Giuffrida, A.; Trapani, G. Novel
Codrugs with GABAergic Activity for Dopamine Delivery in the Brain.
Int. J. Pharm. **2012**, *437*, 221–231.